Materials Today Sustainability 32 (2025) 101234

Contents lists available at ScienceDirect

Materials Today Sustainability

journal homepage: www.journals.elsevier.com/materials-today-sustainability

Development of bio-based flexible polyurethane foams incorporating phase change materials for thermal energy storage applications

Damiano Rossi [a,b,*], Irene Anguillesi [a,b], Emanuele Maccaferri [c], Alekos Ioannis Garivalis [d], Ester D'Accardi [e], Davide Palumbo [e], Maria Michela Dell'Anna [f], Daniele Testi [d,g], Loris Giorgini [c], Maurizia Seggiani [a,b]

[a] Department of Civil and Industrial Engineering, University of Pisa, Largo Lucio Lazzarino 1, 56122, Pisa, Italy
[b] Consorzio Interuniversitario Nazionale per la Scienza e Tecnologia dei Materiali (INSTM), Via Giuseppe Giusti 9, 50121, Florence, Italy
[c] Department of Industrial Chemistry "Toso Montanari", University of Bologna, Viale del Risorgimento 4, 40136, Bologna, Italy
[d] Department of Energy, Systems, Territory and Constructions Engineering, University of Pisa, Largo Lucio Lazzarino 1, 56122, Pisa, Italy
[e] Department of Mechanics, Mathematics and Management, Politecnico di Bari, Via Edoardo Orabona 4, 70125, Bari, Italy
[f] Dipartimento di Ingegneria Civile, Ambientale, del Territorio, Edile e di Chimica, Politecnico di Bari, Via Edoardo Orabona 4, 70125, Bari, Italy
[g] Interdepartmental Research Centre on Energy for Sustainable Development (CIRESS), University of Pisa, Largo Lucio Lazzarino 1, 56122, Pisa, Italy

ARTICLE INFO

Keywords:
Polyurethanes
Foams
Polyols
Phase change materials
Waste cooking oil
PCM

ABSTRACT

The fabrication of innovative polyurethane panels for energy efficiency is increasingly important and should ideally be based on sustainable, non-fossil-based feedstock. In this context, the present work reports the development of sustainable composite panels by incorporating microencapsulated phase change materials (PCMs) into flexible polyurethane (PU) foams, synthesized from a polyol derived from waste cooking oil (WCO) and a partially bio-based isocyanate. The PU-PCM panels achieved energy storage capacity up to 26.2 J/g at a maximum PCM content of 15 phr. Uniform PCM dispersion slightly reduced cell size and increased panel density (from 128 to 157 kg/m^3), thereby enhancing structural support and rigidity while reducing elasticity (compression force deflection up to 234.8 kPa). Fatigue tests confirmed resistance to cyclic loading, with increased dynamic stress and stiffness due to PCM integration. Differential scanning calorimetry showed minimal enthalpy hysteresis (±0.26 J/g) and a stable phase-change temperature (36 ± 0.1 °C), demonstrating resilience to thermal and mechanical stress. Thermal conductivity increased slightly (from 46.15 to 48.44 mW/m·K at 20 °C) due to the silica-based PCM shell, while thermal diffusivity decreased, favouring transient thermal regulation. Fire performance remained unaffected, likely due to the balance between the flammable paraffinic core and the flame-retardant silica shell of PCMs. Overall, bio-based PU-PCM panels show potential for transportation and construction applications owing to their lightweight, insulating, and flame-retardant properties. They offer improved sustainability and thermal-mechanical performance compared to conventional PU panels and flammable PCMs, while supporting circular economy principles by valorising end-of-life WCO.

1. Introduction

Polyurethane foams (PUs) are versatile materials with wide-ranging applications, particularly in the construction and transportation sectors [1]. They are porous copolymers containing urethane bonds (-NHCOO-), typically synthesized through the reaction of polyols (-OH groups) with isocyanates (-NCO groups). PUs are valued for their low density, acoustic insulation, mechanical and vibrational energy dissipation, and excellent thermal insulation, making them attractive for energy-efficient applications [2,3].

Thermal energy-storage capability can be imparted to PUs by incorporating microencapsulated phase change materials (PCMs), forming PU-PCM composites with low thermal conductivity and high thermal inertia [4,5]. These composites are particularly useful for refrigerated transport of temperature-sensitive goods and in transport and building applications, such as wall and ceiling panels, and more recently, for advanced uses including electronics [6] and advanced wearable devices [7,8]. PCMs typically consist of a paraffin core with a

* Corresponding author. Department of Civil and Industrial Engineering, University of Pisa, Largo Lucio Lazzarino 1, 56122, Pisa, Italy.
E-mail address: damiano.rossi@unipi.it (D. Rossi).

https://doi.org/10.1016/j.mtsust.2025.101234
Received 30 July 2025; Received in revised form 17 September 2025; Accepted 4 October 2025
Available online 5 October 2025

polymer shell, absorbing and releasing latent heat during phase transitions to maintain nearly constant temperatures [9]. This stabilizing effect improves temperature regulation and reduces energy consumption by an estimated 15–20 % [10]. PCMs are classified into organic, inorganic, and eutectic types based on their chemical composition and thermal properties. Organic PCMs, such as paraffins and fatty acids, offer high latent heat capacity, stable phase change temperatures, low supercooling, and chemical stability without phase separation. Inorganic PCMs, mainly salt hydrates, provide higher thermal conductivity but often face challenges like phase segregation and supercooling. Eutectic PCMs combine organic and inorganic components to leverage the benefits of both, enhancing thermal performance and stability [9,11].

Research on PU-PCM panels has mainly focused on petroleum-based PU and paraffin-based PCMs. Sarier et al. (2007) first introduced the development of PU-PCM rigid foams incorporating n-hexadecane and n-octadecane PCMs during the polyol-isocyanate polymerization process [12]. Later, similar paraffinic PCMs were used to produce flexible polyurethanes [13]. More recently, rigid PU-PCM panels have been fabricated with PCM loading of 30 wt% n-tetradecane [14] and 20 wt% n-octadecane [15]. To improve thermal and structural properties, PU-PCM panels can be coated with rigid outer layers, creating a sandwich-like composite structure. Castellón et al. (2010) first demonstrated this approach by injecting PCM-enriched rigid PU foam between two metal sheets [16], and subsequent studies have confirmed its effectiveness in producing panels with enhanced load-bearing capacity and thermal energy storage [17–21].

The development of innovative PU-PCM materials for energy savings and efficiency is increasingly necessary and should ideally be supported by sustainable production processes. However, soft and rigid PU panel matrices are still manufactured from petroleum-derived precursors, such as polyether and polyester polyols, combined with aromatic isocyanates such as methylene diphenyl diisocyanates (MDI) and toluene diisocyanates (TDI) [4,12–15]. Since PU accounts for the majority (70–80 wt%) of PU-PCM systems, concerns remain about the actual sustainability of these materials, an issue that deserves further investigation and is the focus of the present work.

The sustainability of PU foams can be enhanced by replacing fossil-based precursors with bio-based alternatives [22]. While the production of green aromatic isocyanates remains challenging, the synthesis of polyols from renewable resources is more feasible [23]. Consequently, extensive research has focused on developing vegetable polyols to partially substitute petroleum-derived ones [24–26]. In this context, our group recently demonstrated the synthesis of rigid [27] and flexible PU [28] using polyols entirely derived from waste cooking oils (WCO) and partially bio-based isocyanates [29], achieving a high bio-based content of approximately 80 wt%. This strategy enables the valorisation of WCO, a problematic and continuously increasing waste stream. In Europe, 0.6–1 Mt of WCO are collected annually, with projections reaching approximately 4 Mt over the next decade [30]. Currently, WCO recycling routes are predominantly limited to biodiesel production, which remains insufficient to meet market demand [31]. Other applications, such as bio-lubricants and animal feed, represent only niche markets compared with the volumes generated [32]. Owing to its growing importance as a renewable polymeric feedstock, the use of WCO for higher value-added products is receiving increasing attention [33]. To date, the only reported effort to produce sustainable PU-PCM panels is by Gama et al. (2018), who employed crude glycerol from biodiesel manufacturing to reduce costs and environmental impact [34]. Building on this, the present study explores the use of WCO-derived PU formulation to develop innovative, sustainable bio-based PU-PCM panels.

PCMs constitute a minor fraction of PU-PCM composite, with their selection dictated by the operating temperature of the intended application [35]. Paraffinic waxes - such as hexadecane [12], n-tetradecane [14], n-octadecane [12,15], and their mixtures - are commonly used cores, with melting points ranging from 5 to 40 °C [36]. Methacrylate copolymers are the predominant shell materials for PCM due to their superior mechanical and thermal properties, chemical compatibility, and ease of fabrication [4,13], while melamine-formaldehyde resins are also frequently employed [4,10].

While the incorporation of PCMs can enhance the thermal and mechanical properties of insulating PU foams [37–40], it may pose challenges due to the flammability of paraffinic or organic cores. Toxicity and environmental concerns also arise from organic cores (paraffins, fatty acids, esters, and alcohols) [41] and polymeric shells (melamine, formaldehyde, and acrylic resins) [35]. Consequently, research has focused on sustainable, non-toxic bio-based PCM cores derived from vegetable oils or animal fats [42–45], organic biochar-derived shells [46,47], and inorganic shells, such as calcium carbonate and silica, which enhance chemical and thermal stability and impart flame-retardant properties [48]. In this context, SiO_2-based PCMs have attracted significant attention due to their unique combination of properties. Although their high thermal conductivity makes them less suitable for insulation applications, SiO_2 shells offer superior mechanical strength, rigidity, and leakage resistance, along with enhanced chemical stability, durability, and low cost [49,50]. Additionally, SiO_2-based shells can encapsulate both water-soluble [51] and oil-soluble PCMs [52]. A key advantage is their inherent fire resistance, eliminating the need for conventional flame-retardant additives - such as magnesium hydroxide, melamine, zinc oxide, or zinc stannates - commonly used in fire-resistant PU foams [4,53].

Building on the potential of silica-based PCMs and their synergy with polyurethane foams, this study evaluates their compatibility with bio-based flexible PU derived from WCO, synthesized according to the method detailed in our previous work [28]. The novel PU-PCM system aims to enhance sustainability and performance, offering a promising solution for transport and construction applications requiring a balance of lightweight properties, mechanical strength, improved thermal management, and reduced flammability compared to conventional petrochemical PU-PCMs.

PU-PCM panels incorporating up to 15 phr of PCM (parts per hundred, by weight) were fabricated and analysed to assess their thermal and mechanical performance. To achieve a comprehensive characterization of the PU-PCM systems, thermal behaviour was evaluated using differential scanning calorimetry (DSC), thermogravimetric analysis (TGA), cone calorimetry, and thermal conductivity measurements, while mechanical performance was examined through compression testing and dynamic mechanical analysis (DMA).

2. Materials and methods

2.1. Materials

A bio-based polyol was synthesized from waste cooking oil (WCO) supplied by Physis srl (Italy) through epoxidation and ring-opening reactions with ethanol, following the procedure outlined in the previous study [28]. The oil has an average molecular weight of 1050 g/mol and a hydroxyl number of 145 mg KOH/g, making it suitable to produce flexible foams.

A partially bio-based polyisocyanate (Desmodur® CQ N7300), derived from pentamethylene diisocyanate (PDI-trimer), with a bio-based carbon content of 68 wt% and an NCO content of 21.9 wt%, was kindly supplied by Covestro AG (Germany).

Triethylene diamine (33 wt%) and dipropylene glycol (67 wt%) (Dabco® 33 LV, Evonik Industries AG, Germany), together with dimethylethanolamine (Dabco® DMEA, Evonik Industries AG, Germany), were employed as gelling and blowing catalysts, respectively. A polysiloxane-polyoxyalkylene block copolymer (Tegostab® BF 2370, Evonik Industries AG, Germany) served as a surfactant and cell stabilizer, while a silicone-free surfactant (Ortegol® 500, Evonik Industries AG, Germany) acted as a cell-opening additive. A tin-based metal catalyst (Kosmos® 19, Evonik Industries AG, Germany) was used as a

crosslinking agent. Distilled water acted as the chemical blowing agent for foam production. All raw materials were used as received, without further purification.

EnFinit® PCM 35CP phase change microcapsules, supplied as a white powder by Encapsys LLC (US), have a paraffinic core material encapsulated in a proprietary silica-based shell. The PCM has a melting point of 35 °C, a latent heat capacity of 167 J/g, and a particle size with 30 wt% retained on a 150 μm sieve. To accurately evaluate the influence of PCM particles on the thermal and mechanical properties of the panels, and to optimize their energy storage capacity, a relatively broad particle size range corresponding to the central cut of the overall PCM distribution was considered. Accordingly, the PCM powder was sieved using a column of Gilson stainless steel meshes arranged in decreasing mesh size. The 125–212 μm fraction was selected for this study, as it represented the largest weight fraction (see Section 3.3 for details). Both coarser and finer fractions were discarded. The coarser fraction contained agglomerates and impurities, and its exclusion ensured more consistent thermal and mechanical performance, thereby reducing variability in foam behaviour and enhancing the overall reliability of the panels. The finer fraction was discarded because it consisted of small particles with a high shell-to-core ratio, which provide lower energy storage per unit weight.

2.2. PU-PCM panels production

The methodology used to produce PU-PCM panels is illustrated in Fig. 1. PCMs were incorporated using a direct integration method, which involves adding the PCM directly to the polyol-isocyanate mixture prior to foaming and curing. This approach is straightforward and cost-effective, particularly suitable for paraffinic core materials [4].

Initially, the bio-based polyol was mixed in a glass beaker with the additives and sieved PCM at varying concentrations (0, 5, 10, and 15 phr; PCM content is based on the total foam mixture, as reported Table 1) (Fig. 1a). The mixture was stirred at 300 rpm for 1 min using a VELP OV725 disperser equipped with D20-S20F-P-R20M probe, appropriate for liquid-solid suspensions (Fig. 1b). The polyisocyanate was then rapidly added, and the mixture was stirred vigorously at 1000 rpm for 1 min. The isocyanate-to-hydroxyl molar ratio (NCO/OH) was maintained at 0.9 for all formulations to obtain flexible PU foams [28] (Fig. 1c). Subsequently, the catalyst was introduced, and the mixture was stirred at 300 rpm for an additional 30 s (Fig. 1d). A total of 170 g of the foam mixture was poured into a closed, rectangular Teflon-coated mould (L = 200 mm × L = 200 mm × H = 30 mm) (Fig. 1e). The mould was sealed, and the foaming process took place at room temperature (18 °C) for 24 h in a controlled volume (Fig. 1f). The PU-PCM foam was then removed from the mould and post-cured in a ventilated oven at 70 °C for 8 h (Fig. 1g). The resulting foams, containing 0, 5, 10, 15 phr PCM, were designated P0, P5, P10, and P15, respectively, and were subsequently subjected to characterization (Fig. 1h). PCM Concentrations above 15 phr may result in foams that are too fragile and lack flexibility; therefore, they were not considered in this study.

The concentrations of reagents and additives, based on 100 g of polyol, are reported in Table 1 and were determined according to our previous study [28].

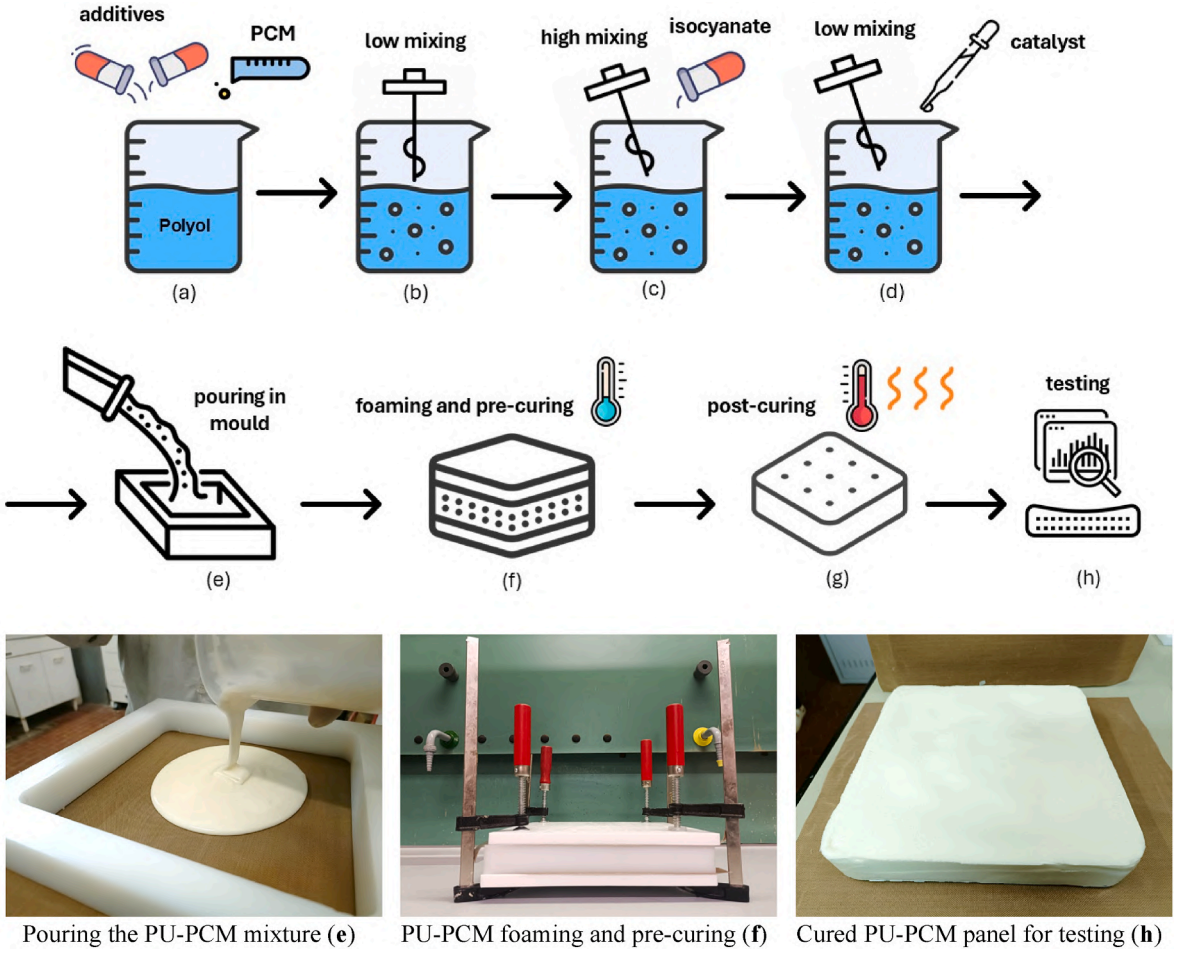

Fig. 1. Scheme and some photos of PU-PCM panel preparation. Preparation of polyol, additives, and PCM formulation (**a**). Polyol, additives, and PCM low mixing (**b**). Isocyanate addition and rapid mixing (**c**). Catalyst addition and low mixing (**d**). Pouring the PU-PCM mixture in the mould (**e**). PU-PCM foaming and pre-curing (**f**). PU-PCM post-curing (**g**). Final cured PU-PCM panel ready for testing (**h**).

Table 1
Formulations of PU-PCM panels with different PCM content (P0, P5, P10, and P15). phr stands for 'parts per hundred': grams of PCM per 100 g of the total foam mixture, including polyol, Desmodur, and other additives.

PU-PCM	Polyol (g)	Desmodur® CQ N7300 (g)	Tegostab® 2370 (g)	Dabco® 33 L V (g)	Dabco® DMEA (g)	Ortegol® 500 (g)	Kosmos 19 (g)	Water (g)	PCM (g)
P0	100.0	123.5	1.1	0.36	0.8	1.5	1.5	4.0	0.0
P5									11.6
P10									23.3
P15									34.9

2.3. Panel characterization

2.3.1. Thermal analysis

Differential scanning calorimetry (DSC) was used to determine the energy storage capacity and the effective encapsulation of PCM incorporated within the developed panels. Measurements were performed using a DSC 6000 (PerkinElmer Inc, US), which has a temperature accuracy of ±0.1 °C and temperature precision of ±0.02 °C. Approximately 15 mg of each sample was placed in an aluminium pan and subjected to heating-cooling-heating cycles from −20 to 70 °C at a rate of 1 and 10 °C/min. The effective PCM content ($\%_{PCM}$) incorporated into the foam was determined as follows:

$$\%_{PCM} = \frac{\Delta H_P}{\Delta H_{PCM}} \cdot 100 \quad (1)$$

where, ΔH_P and ΔH_{PCM} are the melting latent heats of the panels and PCM, respectively. $\%_{PCM}$ represents the mean value of five replicates.

The thermal stability of the panels was evaluated by thermogravimetric analysis (TGA) using an STA 2500 Regulus (Netzsch BV & Co Holding KG, Germany), which has a weight accuracy of ±0.03 μg and a temperature precision of ±0.3 °C. Samples of about 5 mg were heated in a platinum pan from room temperature to 900 °C at a rate of 1 °C/min under a nitrogen flow of 20 mL/min.

Thermal conductivity (λ) of the panels was measured using a TPS3500 (Hot Disk AB, Sweden) in bulk module, following the ISO/FDIS 22007-2 standard. Rectangular samples (L = 50 mm × L = 50 mm × H = 30 mm) were extracted from the central portion of the post-cured panels. Measurements were performed at 20, 25, 30, 35, 40, 45, and 50 °C ± 1 °C using a 10 mm sensor. Mean thermal conductivity values were calculated from five readings per specimen. The instrument provides thermal conductivity accuracy <5 % and a thermal conductivity precision <0.11 %.

Fire behaviour of the panels was evaluated using a cone-calorimeter apparatus (Fire Testing Technology Ltd, UK) under heat fluxes of 25 and 35 kW/m^2, simulating small-to-medium fire scenarios, both with and without ignition triggered by an electric spark. Specimens measured L = 100 mm × L = 100 mm, in accordance with ASTM E1354-17, with thickness ranging from 7 to 8 mm, and were taken from the central portion of the panels to avoid surfaces in contact with the mould, which may contain defects. The apparatus was designed to operate in accordance with ISO 5660 and calibrated prior to testing to ensure data reliability.

2.3.2. Fourier transform infrared spectroscopy (FTIR)

FTIR spectra were recorded in attenuated total reflectance (ATR) mode using a Cary 630 FTIR spectrometer (Agilent Technologies Inc, US) over a wavenumber range of 500–4000 cm^{-1} with a resolution of 2 cm^{-1} (wavenumber accuracy ± 0.05 cm^{-1}; wavenumber reproducibility ± 0.005 cm^{-1}). The analysis was performed on the panels to verify the completion of polyurethane synthesis and assess the chemical affinity between PCM and PU.

2.3.3. Mechanical analysis

Compression force-deflection (CFD) tests were performed at 20 °C on the fabricated panels using a Qasar 10 compression testing machine (Galdabini S.p.A., Italy) equipped with a 10 kN load cell. In accordance with ASTM D3574-C, rectangular samples (L = 50 mm × L = 50 mm × H = 30 mm) were obtained by cutting larger post-cured panels. Each sample was pre-compressed twice to 75 % of its initial height at a speed of 250 mm/min. After a 6 min rest period, the sample height was measured under a residual load of 140 Pa. Finally, the samples were then compressed to 50 % of their height at a speed of 50 mm/min, and the load ($\sigma_{50\ \%}$) after 60 s was recorded. $\sigma_{50\ \%}$ represents the mean value of five replicates.

Dynamic mechanical analysis (DMA) was conducted to evaluate the viscoelastic behaviour and the glass transition temperature (T_g) of the panels. Foam disks (14 mm in diameter, 10 mm thick) were cut from the panels and tested in compression mode using a DMA 303 Eplexor (Netzsch BV & Co Holding KG, Germany), which provides a maximum controlled amplitude of ±2.5 mm, a maximum static deformation of ±15 mm, and a position resolution of ±1 nm. The analysis spanned a temperature range from −70 to 120 °C, with a heating rate of 2 °C/min at a frequency of 1 Hz and dynamic deformation of 70 μm. The same foam disk samples were used to assess the panels' ability panels to withstand cyclic loading at 20 and 50 °C. Fatigue tests were conducted by adapting the ASTM D3574-11 standard on a DMA apparatus. Tests were performed for 2 h at a frequency of 70 cycles per minute, recording the load required to induce dynamic deformation corresponding to 25 % of the sample thickness. Five replicates were performed for each sample.

2.3.4. Density and morphological analysis

The density of the flexible panels was measured according to ISO 845:2006 using rectangular samples (L = 50 mm × L = 50 mm × H = 30 mm) cut from the panels. The reported value corresponds to the mean value of five replicates.

Cell sizes and foam morphology were examined using scanning electron microscopy (SEM) EM-30N (COXEM Co Ltd, South Korea) with a spatial resolution <5 nm. Samples were fractured in liquid nitrogen, and the surfaces were coated with a thin gold layer using an S150B sputter coater (Edwards Ltd, UK). In addition to SEM, optical microscopy was performed using a S9i stereo microscope (Leica AG, Germany) equipped with a CCD camera.

3. Results and discussions

3.1. Thermal analysis

Fig. 2 shows the DSC curves of the produced panels at different PCM concentrations, while Table 2 reports the corresponding effective incorporation ($\%_{PCM}$) within the PU foam. The absence of exothermic peaks in the P0 curve confirms the completion of the post-curing process and the full crosslinking of polyurethane [28]. Moreover, the flat profile of P0 does not exhibit endothermic peaks in the 30–40 °C range, typically associated with the evaporation of moisture absorbed by open-cell structures [54].

The melting temperature of the pure PCM (T_m = 34.8 °C) agrees with the value reported in the datasheet and closely matches the melting temperature measured in the PCM-loaded panels (T_m = 34.2 °C). This indicates that the PU foam can incorporate the PCM without hindering its ability to undergo phase change and volume expansion during

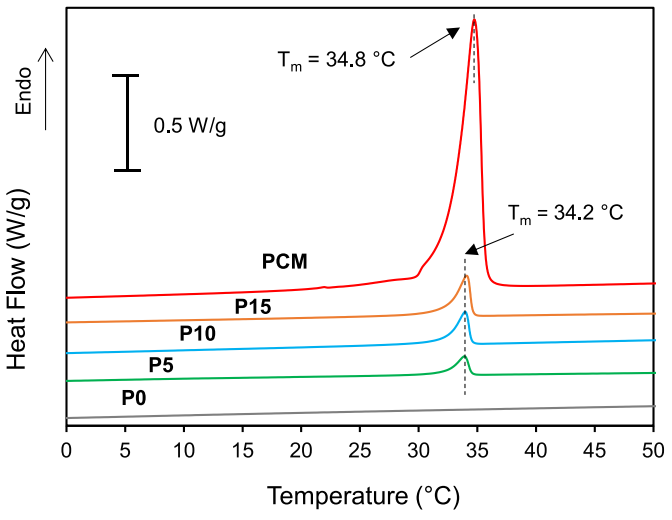

Fig. 2. DSC thermograms of panels. Scan rate = 1 °C/min under a nitrogen flow. 2nd heating. Average curves based on 5 replicates.

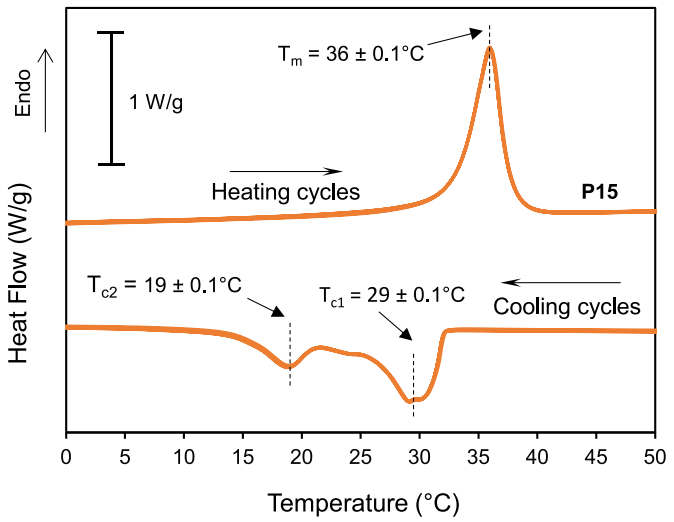

Fig. 3. DSC thermograms of P15 panels at scan rate of 10 °C/min under nitrogen flow over 100 heating-cooling cycles.

Table 2
Nominal and effective PCM concentrations in panels. Mean values ± standard deviation based on 5 replicates.

Sample	Nominal PCM (phr)	Nominal PCM (wt. %)	Effective PCM (wt.%) (Eq. (1))
P0	0	0	0
P5	5	4.8	5.2 ± 2.3
P10	10	9.1	8.5 ± 1.7
P15	15	13.0	14.0 ± 1.1

ΔH_{PCM} = 187 J/g.

melting. All PU-PCM panels exhibit signals attributable to the PCM melting process, and the presence of a single sharp peak indicates a relatively uniform distribution of the core paraffin wax. Furthermore, as the PCM content increases from 5 to 15 phr, the specific enthalpy stored during heating rises from ΔH_P = 9.7 J/g to ΔH_P = 26.2 J/g, confirming the enhanced energy storage capacity with higher PCM loading. These enthalpy values are in line with those reported by Galvagnini et al. (2022), Mahajan et al. (2023), and Fredi et al. (2024) for petroleum-based polyurethane foams and polymer-based PCMs with paraffinic cores at comparable PCM contents [14,19,20].

The calculated latent heat of the pure PCM (ΔH_{PCM} = 187 J/g) is slightly higher than the datasheet value. This difference is attributed to the sieving process, which removed the top and bottom particle fractions that are rich in impurities and shell fragments. It is important to note that the reported energy storage capacities exclusively refer exclusively to the latent heat measured by DSC analysis. The measurement is conducted within a temperature range that is specifically selected to encompass the entirety of the PCM melting and solidification processes. Conversely, the additional sensible heat capacity that is present within the temperature range under investigation is not considered.

The encapsulation efficiency ($\%_{PCM}$), calculated using Eq. (1), is consistent with the theoretical PCM concentration in the panels (Table 2). The standard deviations decrease from 2.3 to 1.1 wt% as the PCM concentration increases, indicating a segregation effect that is more pronounced at lower concentrations. Lower precursor viscosity at lower PCM content (P5) compared to higher content (P15) promotes greater particle stratification due to buoyancy-driven separation [9,55].

To assess the thermal resilience of the PU-PCM composites, the panel with the highest PCM content (P15) was subjected to 100 consecutive heating-cooling cycles at a high rate of 10 °C/min. The DSC thermograms shown in Fig. 3 display overlapping curves and negligible enthalpy hysteresis (ΔH_{P15_cycled} = 26.2 ± 0.26 J/g), which is typically associated to progressive leakage of molten PCM after repeated thermal loading. The leakage of the paraffinic core from the PCM alters both the magnitude and the position of the endothermic and exothermic peaks, since the PCM shell slightly affects the kinetics of the phase transition [14,19,56]. These results demonstrate that the designed panels can withstand thermal stress without compromising their thermal energy storage capacity. The observed stability of melting temperatures could be particularly beneficial for applications requiring precise temperature control, such as temperature-sensitive product packaging.

The slightly higher melting temperature (T_m = 36 ± 0.1 °C) is attributed to the higher heating rate (10 °C/min) and the different kinetic response of the system, compared to the melting temperature obtained at the lower scan rate of 1 °C/min (T_m = 34.8 °C, Fig. 2). However, as expected, the enthalpy associated with these peaks remains essentially unchanged, at approximately 26.2 J/g. The two peaks observed in the cooling curves of Fig. 3 (T_{c1} = 29 ± 0.1 °C and T_{c2} = 19 ± 0.1 °C) reflect the paraffinic nature of core material, likely resulting from the rotator phase transition of n-alkanes [57].

Thermogravimetric analysis of the PCM displays a characteristic bimodal degradation profile, with two main degradation peaks at approximately 230 and 375 °C, corresponding to the thermal decomposition of the alkanes-based core [58] and the silica-based shell, respectively (Fig. 4a–b) [49,50]. A small residue of approximately 1 wt % is attributed to the presence of silica from the PCM shell. No consistent degradation trends were observed as a function of the PCM content in the PU foam. This is due to the small sample size (5 mg) used in each TGA measurement, which does not capture the heterogeneity of the PU-PCM composite system. In fact, experimental variability among multiple samples of the same formulation is comparable to the differences observed between different formulations. All thermograms for the panel samples fall within the grey boundaries in Fig. 4a–b; the average profile is therefore reported as a black line.

All panel samples showed no thermal events below 120 °C, a temperature range typically associated with moisture evaporation or the release of residual unreacted volatile precursors and additives. Thermal stability was maintained up to 200 °C. Above this temperature, three main decomposition stages were identified. The first event, around 250 °C, corresponds to the degradation of the hard segment and the cleavage of urethane bonds [27,59,60]. The main weight loss occurred between 300 °C and 500 °C, with two distinct peaks at 375 °C and 440 °C, attributed to the overlapping degradation of the soft segments in the PU foam and the aliphatic chains of both the isocyanate and polyol components [23].

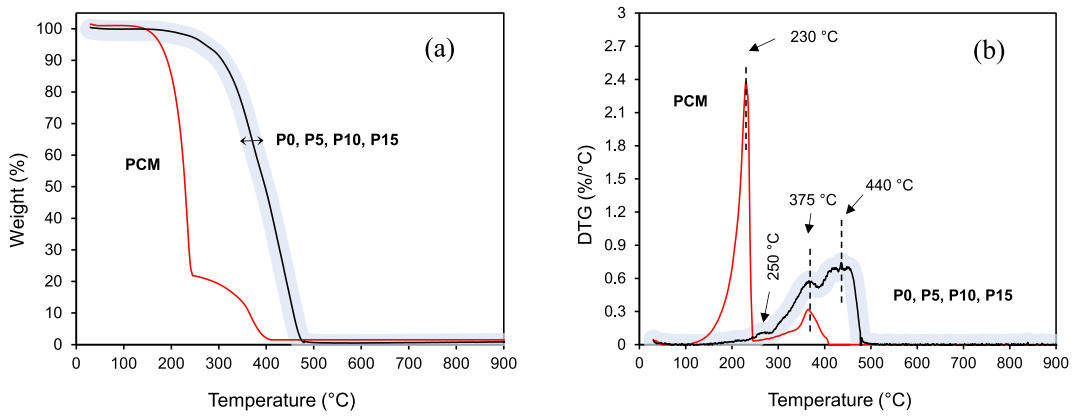

Fig. 4. TG (**a**) and DTG (**b**) thermograms of panels. Scan rate = 1 °C/min under nitrogen flow. Average curves based on 5 replicates. P0, P5, P10, and P15 show similar profiles all contained within the grey region. The average black line indicates their average value.

Notably, the degradation behaviour of the virgin foam (P0) closely matches that of the PCM-containing foams. This similarity is likely due to the complete encapsulation of the PCM within the foam, which protects the microcapsules and attenuates the appearance of the characteristic degradation peaks of the paraffinic core. These findings indicate that, although PCM microcapsules possess lower intrinsic thermal stability compared to the virgin PU foam (P0), unlike those with melamine-formaldehyde shells [19,20], they do not compromise the overall thermal stability of the PU-PCM panels. This behaviour may be ascribed to the strong affinity between the hydroxyl groups of the silica-based shell and isocyanate groups, which can undergo chemical reactions [61]. This interpretation is further supported by subsequent FTIR analyses.

3.2. Fourier transform infrared spectroscopy

The virgin panel (P0) exhibited the typical FTIR spectrum of post-cured PU foam, confirming the completion of the polyaddition reactions between polyol and isocyanate (Fig. 5). This is demonstrated by the presence of urethane bond signals: a broad peak at 3360 cm^{-1} (N-H stretching), a peak at 1530 cm^{-1} (N-H in-plane bending), a peak at 760 cm^{-1} (N-H wagging), and a peak at 1230 cm^{-1} (C-N stretching) [27,62]. In addition, the disappearance of the band at 2260 cm^{-1}, associated with the isocyanate bond (N=C=O), along with the appearance of a peak at 1690 cm^{-1} corresponding to the C=O bond in urethane, confirms that the isocyanate groups have fully reacted with the hydroxyl groups of the polyols to form urethane bonds [63–65]. The bands at 2930 cm^{-1} and 2850 cm^{-1} correspond to the asymmetric and symmetric stretching vibrations of -CH_2 groups, respectively, associated with the aliphatic chains of both polyol and isocyanate components [66].

The PU-PCM foams exhibited FTIR spectra identical to those of the virgin P0, supporting the hypothesis that PCM particles are fully encapsulated and shielded by the polyurethane matrix, rendering their specific signals undetectable by ATR-FTIR. The similarity of the spectra among all panel samples further demonstrates that PCM and PU do not chemically interact and are physically embedded.

The PCM spectrum exhibits the same peaks at 2930 cm^{-1} and 2850 cm^{-1}, corresponding to -CH_2 stretching vibrations of the paraffinic core. Additional bands in the 800-1730 cm^{-1} region are likely associated with Si-CH_3 and Si-O-Si vibrations, originating from the silica-based shell [66,67]. The band at 1730 cm^{-1} indicates the presence of C=O bonds, possibly from long-chain esters within the organic core of the PCM. The peak at 720 cm^{-1} (zoomed-in section of the spectrum) is attributed to the in-plane -CH_2 rocking vibration [68], characteristic of long-chain hydrocarbons such as paraffinic structures. This vibration is commonly associated with the ordered packing of methylene (-CH_2-) groups in crystalline or semi-crystalline regions of aliphatic chains,

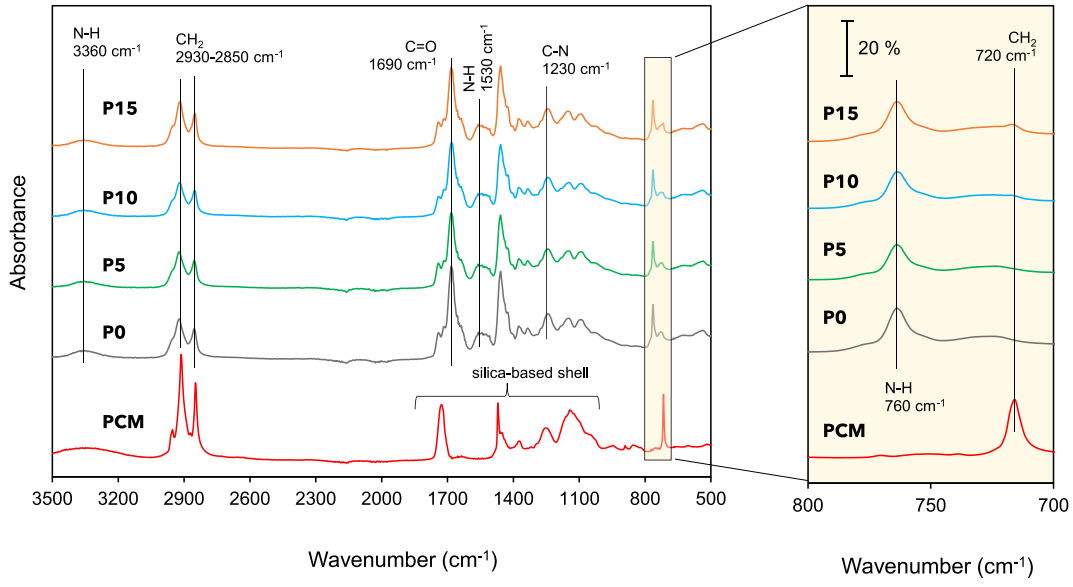

Fig. 5. FTIR-ATR spectra of panels and PCM. Wavenumber range of 500–4000 cm^{-1}; resolution of 4 cm^{-1}. Average curves based on 5 replicates.

which largely constitute the PCM core. Notably, this peak increases in intensity with increasing PCM content.

3.3. Morphology

Fig. 6 shows the particle size distributions of the commercial PCM after sieving. The 125–212 μm fraction accounts for the largest weight percentage (54 wt%) and is mainly composed of spherical particles with smaller satellites adhered to their surface. ImageJ software was used to determine the size of the PCM particles and to analyse the PU-PCM cell structure.

Each post-cured panel shown in Fig. 1h was sectioned into rectangular specimens (L = 50 mm × L = 50 mm × H = 30 mm, Fig. 7a). The samples were cryo-fractured, and their cross-sections were examined via SEM to assess the PU-PCM morphology and the dispersion of PCMs within the polyurethane matrix (Fig. 7b–g). The SEM micrographs of P0 (Fig. 7b) revealed a well-defined cellular morphology composed of both open and closed-cells, consistent with the study focus and the use of the cell-opening agent Ortegol® 500. The cells exhibited a regular shape with a relatively narrow size distribution (200–500 μm), in agreement with the findings of Rossi et al., 2025 [28]. PCM particles tended to accumulate between the cells, particularly at strut-joints connecting three or more cells (Fig. 7d–f) slightly distorting the polyhedral cell morphology and reducing cell dimension (100–450 μm). This behaviour is related to the nucleating effect of PCM particles during polyurethane crosslinking [69]. Similar localized accumulation of PCM particles, enclosed within the PU matrix at the inner junction of cell boundaries, has also been reported by Mahajan et al. (2023) [14].

The presence of embedded PCM within PU struts supports previous thermal and FTIR analyses. This affinity between PCM and PU benefits overall composite integrity but also hinder the foaming process. This is evidenced by the interface between PCM and PU, which exhibits microporosity (1–5 μm), characterized by incompletely developed cells (Fig. 7g). Since silica particles are partially surface-terminated with Si-OH groups, they can interfere with polyurethane formation. A possible explanation is that silica reduces the extent of the foaming by reacting through its OH groups with a part of the isocyanate, thereby lowering the availability of isocyanate groups for reaction with the polyol and water during foaming [61,70]. This effect was also confirmed by Frances et al. (2014), who investigated the influence of silica nanoparticles on the polyurethane foaming process and foam properties [71].

Stereo microscope images of P0 (Fig. 8a) and P15 (Fig. 8b) confirm the uniform distribution of PCM microcapsules within the foam matrix. The PCM microcapsules appear evenly dispersed across the cell surfaces, indicating their effective incorporation into the PU foam and their excellent compatibility.

Interestingly, the P5 samples exhibited upper regions slightly richer in PCM than the lower regions, suggesting segregation towards the top due to the lower density of PCM relative to the precursors. This observation is consistent previous reports of particle segregation at low PCM content (Table 2). The density of the precursor mixture prior to foaming, measured with a pycnometer, was 1.15 g/cm^3, higher than the typical density of paraffinic PCMs (<1 g/cm^3) [9].

3.4. Mechanical characterization

Fig. 9a presents the density trend (at 20 °C) of the designed panels as function of the PCM content. The nominal density (ρ_n) corresponds to the density of the mixture prior to foaming (Fig. 9b), while the total density (ρ_t) represents the final density of the rectangular panel portion after post-curing (Fig. 9c). The bulk density (ρ_b) refers to the homogeneous density of the panel portion after the removing the upper and bottom layers (3 mm thickness each) as well as the edges in contact with the Teflon-coated mould (Fig. 9c). As expected, $\rho_n > \rho_t$ in P0, a difference attributed to the gas released during foaming. In contrast, $\rho_t \gtrsim \rho_b$, with only minor differences due to the removal of the denser cellular structure formed near the Teflon mould.

The nominal density ρ_n increased with the PCM content (from P0 to P15). Interestingly, in the PCM-containing samples, $\rho_n < \rho_t$, confirming that the presence of silica-based PCM inhibits the foaming process, resulting in more compact and rigid structures [61,70]. Consequently, $\rho_t > \rho_b$ with a larger deviation than P0, reflecting the removal of the outer layers enricher in PCM.

The bulk density (ρ_b) ranged from 128 to 157 kg/m^3 (a 23 % increase), which is consistent with flexible polyurethane foams used in insulation and packaging applications, requiring load-bearing capacity [72]. The density of the virgin panel P0 is higher than that reported by Rossi et al. (2025) for the same precursors (128 kg/m^3 vs. 86 kg/m^3) [28]. This discrepancy is attributed to different temperatures used during the foaming stage (18 °C vs. 25 °C). The higher temperature in the previous study likely enhanced foam expansion and promoted cell wall rupture, leading to a greater fraction of open cells [73].

It is well established that PCM phase transitions are accompanied by a general volume increase [9]. However, this effect is usually negligible and cannot be detected in real time by SEM analysis, as the instrument is not equipped with temperature control. To confirm this, bulk density measurements were carried out after preconditioning the panels in an oven at 50 °C > T_m. The values matched those obtained at room temperature (20 °C < T_m), confirming that the phase transition does not alter the morphology or dimensions of the developed panels.

Fig. 10 reports the compression force deflection (CFD) values measured at 20 °C. These values were markedly affected by the PCM content incorporated into the foam. The panels exhibited CFD values ranging from 85.5 kPa (P0) to 234.8 kPa (P15), corresponding to an almost threefold increase in compressive resistance with higher PCM content. The presence of rigid inclusions enhances stiffness in a nearly

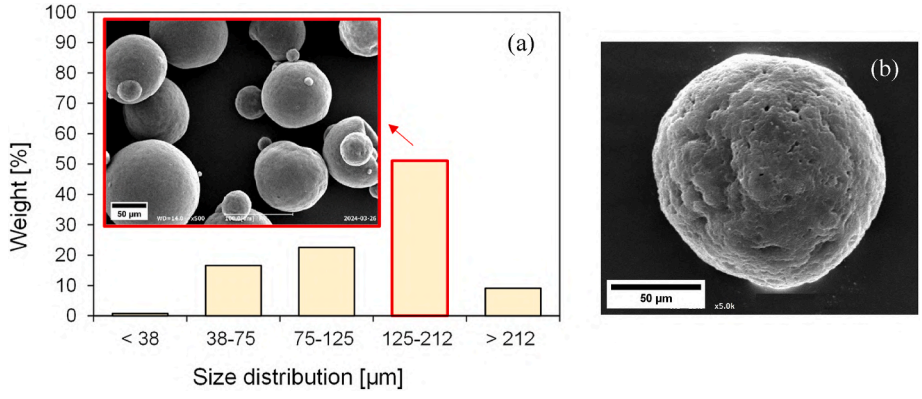

Fig. 6. Particle size distribution of commercial EnFinit® PCM 35CP (**a**). PCM particle (**b**). The 125–212 μm size range constitutes the largest weight fraction (54 wt%).

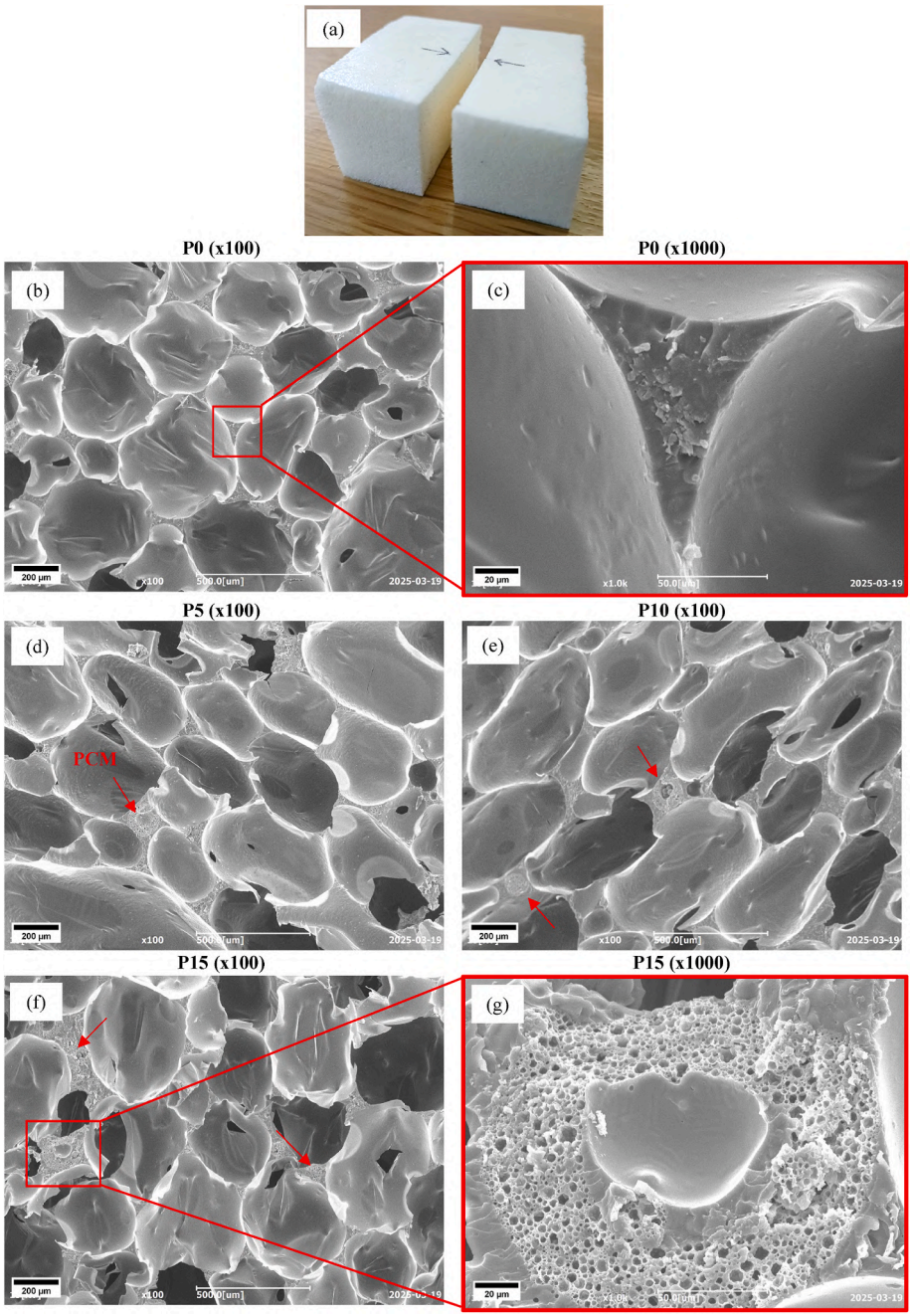

Fig. 7. Cryo-fractured portion of panels (L = 50 mm × L = 50 mm × H = 30 mm) (**a**). SEM images of P0 at different magnifications (**b-c**), P5 (**d**), P10 (**e**), and P15 (**f-g**). Red rows indicate PCM particles accumulated at the strut joints connecting three or more cells.

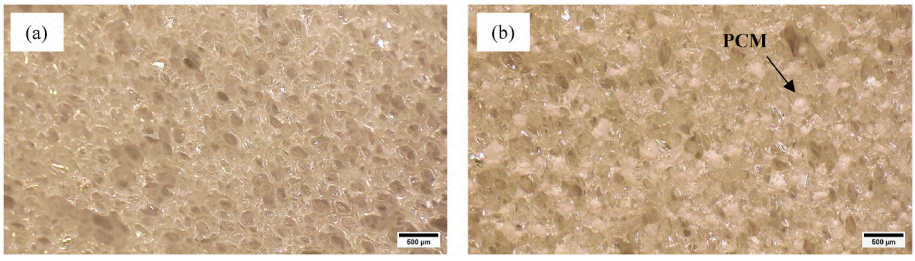

Fig. 8. Stereo microscope images of P0 (**a**) and P15 (**b**). PCM particles in P15 appear evenly dispersed into the PU foam matrix.

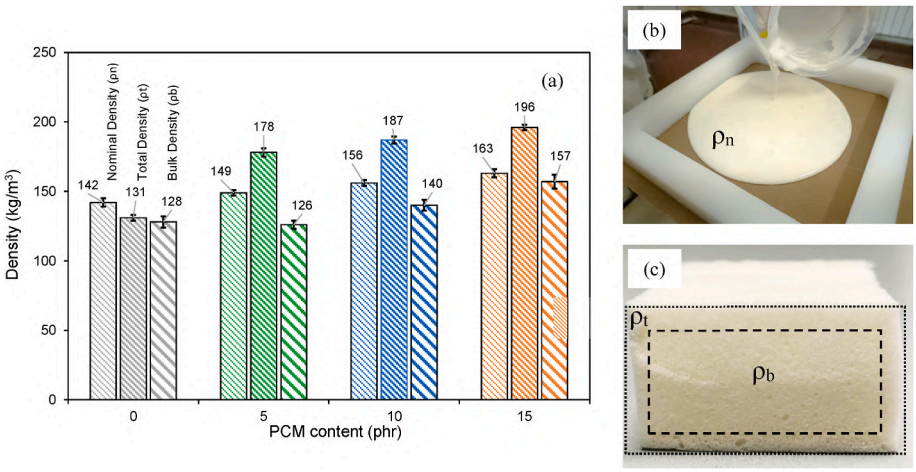

Fig. 9. Nominal density (ρ_n), total density (ρ_t), and bulk density (ρ_b) as function of nominal PCM content at 20 °C (**a**). Mean values ± standard deviation based on 5 replicates. Mixture before foaming and ρ_n (**b**). Portion of panel (L = 50 mm × L = 50 mm × H = 30 mm) and contour used for the determination of ρ_t and ρ_b (**c**).

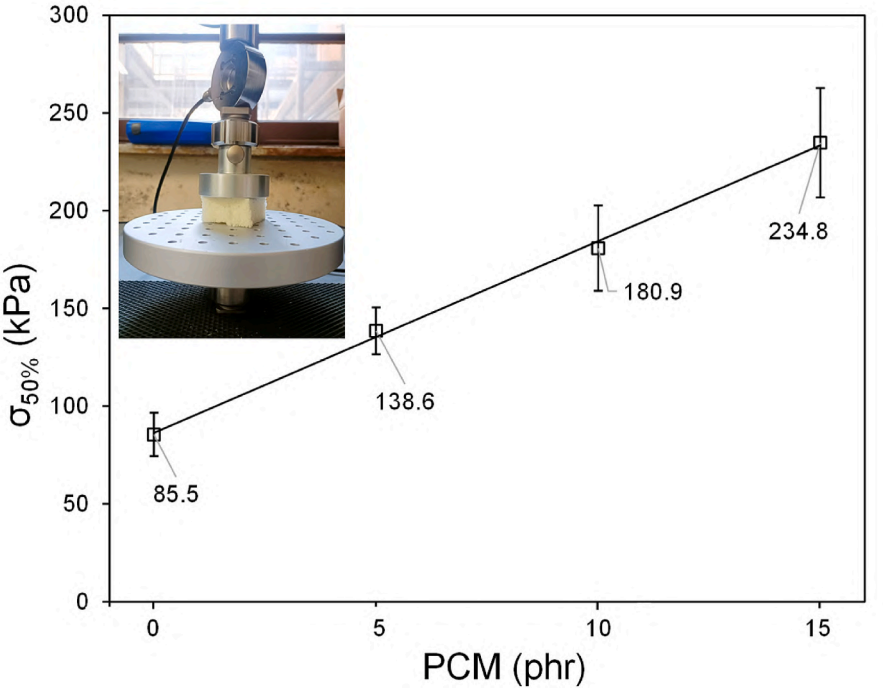

Fig. 10. Compression force deflection (CFD) test (ASTM D3574-C) performed at 20 °C on rectangular samples (L = 50 mm × L = 50 mm × H = 30 mm). $\sigma_{50\ \%}$ as function of PCM content. Mean values ± standard deviation based on 5 replicates.

proportional manner, since the particles act as effective reinforcements within the polymer network. This trend is expected, as the PCM occupies space within the polymeric struts, thereby reducing cell dimension (Fig. 7). A greater number of smaller cells enhances the ability to withstand external loads, since the increased strut density per unit area improves structural support. Consequently, the panels display reduced elasticity but increased strength and rigidity [15,74]. These findings are consistent with the results of Galvagnini et al. (2022) and Fredi et al. (2024), who reported increased stiffness accompanied by a marked reduction in strain at failure in three-point bending tests [19,20]. Comparable trends were also observed in PU-PCM composites examined by Gama et al. (2018), Vatankhah et al. (2022), and Mahajan et al. (2023) under uniaxial compression [14,15,34].

The relatively high CFD values obtained highlight the suitability of the panels for insulating and reinforcing structural components in automotive and building applications, where high stiffness (CFD >200 kPa) is required [72]. Furthermore, the results demonstrate that tailoring the PCM concentration in the initial mixture provides a straightforward means to customize the foam's stiffness for specific application needs.

Fig. 11 presents the DMA results of the panels. The dynamic storage modulus (E′) curves exhibit characteristic trends that correlate with both PCM content and CFD values. Within the operational temperature range of the panels (from −10 to 50 °C), higher PCM concentrations yield foams with generally greater E' values, indicating increased stiffness and enhanced resistance to dynamic deformation. The higher density and stiffness imparted by PCM incorporation are also expected to improve acoustic performance, contributing to sound absorption and vibration damping.

The peak associated with the motion of the side chains (β-transition)

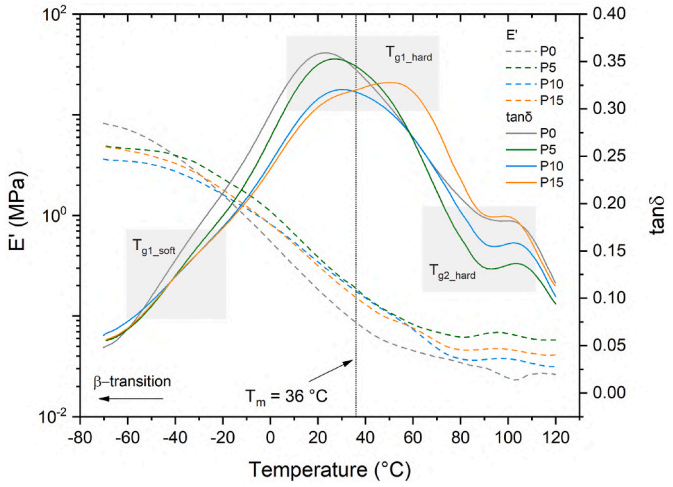

Fig. 11. Dynamic mechanical analysis (DMA) test performed on foam disks (14 mm in diameter, 10 mm thick). E′ and tanδ as a function of temperature (from −70 to 120 °C); heating rate of 2 °C/min at a frequency of 1 Hz and dynamic deformation of 70 μm. Average curves based on 5 replicates.

[75], typically observed below −120 °C in the loss factor (tanδ) [28], is absent within the studied temperature range. In all formulations, the glass transition of the soft segments (T_{g1_soft}) appears as a small shoulder preceding the primary glass transition of the hard segments (T_{g1_hard}) [76,77]. This behaviour suggests a high crosslinking density and good miscibility between the two phase domains, likely promoted by hydrogen bonding interactions between the -NH- groups in the soft segments and C=O groups in the hard segments [63–65].

While T_{g1_soft} remains nearly unchanged (ranging from −40 °C in P0 to −35 °C in P15), T_{g1_hard} shifts to higher temperatures (from 20 °C in P0 to 60 °C in P15). This upward shift is attributed to the reinforcing effect of the PCM shell, which increases rigidity and restricts hard-segment relaxation, thereby elevating their glass transition temperature. A secondary, minor hard-segment transition (T_{g2_hard}) remains essentially unaffected by PCM content [28].

Notably, no shoulders or peaks appear at the PCM melting temperature (T_m = 36 °C), confirming that the paraffinic PCM core is effectively encapsulated within a rigid, non-melting shell. This finding further supports the absence of leakage, which would otherwise soften the material and reduce the glass transition peaks [15,19,20].

Polyurethane insulating foams are widely used in applications involving repeated loading cycles, such as packaging and cushioning. Fig. 12 illustrates the evolution of dynamic tensile stress over multiple loading cycles at 25 % deformation for the virgin panel (P0) and the panel with the highest PCM content (P15). For P0, load-bearing capacity and dynamic deformation resistance progressively decrease with increasing cycle number and temperature (from 20 to 50 °C). This behaviour is attributed, respectively, to partial damage of the cellular structure caused by cyclic loading and to polymer chain relaxation occurring at $T > T_{g1\_hard}$ [2,78]. At these temperatures, the polymer chains exhibit high mobility, leading to rapid relaxation, which can reduce the accumulation of localized stresses but also compromise the integrity of the foam's cellular structure.

Incorporation of PCM (P15) results in higher dynamic stress compared to P0 at both 20 and 50 °C, due to the increased stiffness imparted by the PCM. Accordingly, the slopes of the curves in Fig. 12, representing the rate of polymer chain relaxation under cyclic loading, become steeper with increasing PCM content and decreasing temperature [2].

Fatigue tests were further conducted on P15 by subjecting samples to 100 consecutive heating-cooling DSC cycles at a high rate (10 °C/min) to evaluate potential shell ruptures leading to PCM leakage and/or foam-PCM detachment. The resulting thermograms closely overlap with those in Fig. 3, showing negligible enthalpy hysteresis ($\Delta H'_{P15\_cycled}$ = 25.9 ± 0.21 J/g) and unchanged melting and cooling temperatures (T'_m = 35.9 ± 0.1 °C, T'_{c1} = 29 ± 0.1 °C, T'_{c2} = 19 ± 0.1 °C). These results confirm that the designed panels can withstand thermal stress without compromising thermal energy storage performance, even after repeated mechanical loading.

3.5. Thermal conductivity

Fig. 13 presents the experimental thermal conductivity (λ) of the virgin panel (P0) and the PU-PCM panel with the highest PCM content (P15). As expected for insulating materials, P0 exhibits a linear increase in λ with temperature, ranging from 46.15 to 47.81 mW/m·K [4,13], consistent with values reported for open-cell insulating panels [4]. The P15 panel exhibits a slightly higher thermal conductivity (48.44–48.58 mW/m·K) compared to P0, which is attributed to the presence of the conductive silica-based PCM shell [49,50]. However, this modest

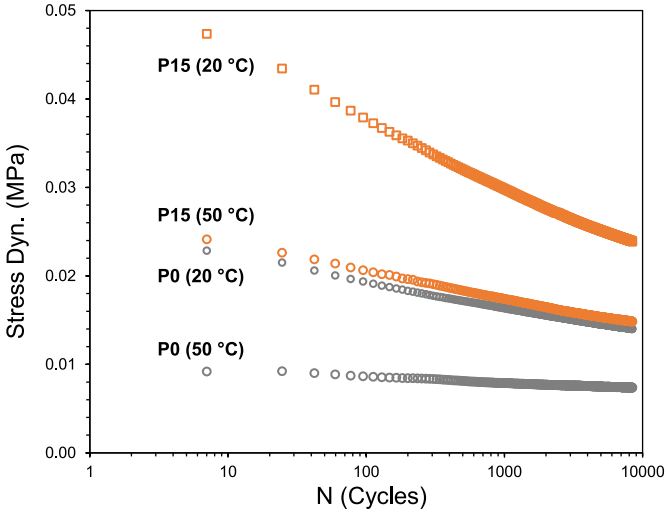

Fig. 12. Dynamic mechanical analysis (DMA) fatigue tests (ASTM D3574-11) performed on P0 and P15 foam disks (14 mm in diameter, 10 mm thick) at 20 °C and 50 °C. Dynamic stress required to induce dynamic deformation corresponding to 25 % of the sample thickness. 2 h repeated cycles (70 cycles per minute). Average curves based on 5 replicates.

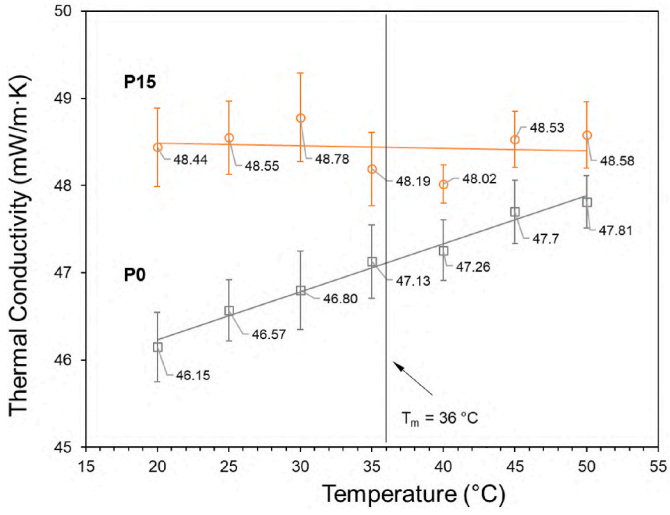

Fig. 13. Thermal conductivity (λ) of P0 and P15 as function of temperature (from 20 °C to 50 °C) based on ISO/FDIS 22007-2 standard and rectangular samples (L = 50 mm × L = 50 mm × H = 30 mm). Mean values ± standard deviation based on 5 replicates.

increase does not compromise the overall insulating performance of the panel. Notably, the nearly constant λ values measured for P15 with increasing temperature likely result from two opposing effects: the intrinsic positive temperature dependence of thermal conductivity is counterbalanced by a reduction occurring near the PCM solid-liquid phase transition ($T_m = 36$ °C) [37–40].

PU-PCM panels are particularly advantageous under transient thermal conditions, as the presence of PCMs attenuates temperature peaks and helps maintain stable thermal conditions over short time spans. The improvement of transient thermal performance of the insulating panel with PCM can be assessed through the thermal diffusivity ($\alpha = \lambda / \rho_b \overline{c_p}$) of the material. When PCM is incorporated, the composite exhibits averaged thermal properties. As shown in Fig. 13, λ changes only marginally between P0 and P15. In contrast, the equivalent specific heat capacity ($\overline{c_p}$) of P15 is expected to be substantially higher than that of P0, especially within the phase transition range. This increase is attributed to the latent heat storage/release ($\Delta H_{PCM} = 187$ J/g), which is incorporated into the $\overline{c_p}$ term along with the sensible heat capacity of the composite foam [79]. Furthermore, bulk density increases from $\rho_b = 128$ kg/m^3 (P0) to 157 kg/m^3 (P15). The combined increase in $\overline{c_p}$ and ρ_b reduces the thermal diffusivity of P15 compared to P0. A lower α corresponds to a slower thermal response, meaning that P15 delays the propagation of the thermal front compared to P0. Consequently, the PCM-loaded panel enhances the ability of the system to dampen rapid temperature fluctuations and maintain more stable thermal conditions in the insulated environment.

3.6. Cone calorimetry

The fire behaviour of both P0 and P15 was evaluated by cone calorimetry under various conditions simulating small-to-medium fire scenarios (35 and 25 kW/m^2), with and without an ignition trigger (Fig. 14).

All samples sustained combustion under a heat flux of 35 kW/m^2. This outcome is expected due to the relatively high flammability of polyurethanes [80], as also indicated by their very short time to ignition - typically a few seconds in standard conditions [81]. The heat release rate (HRR) analysis revealed similar heat production profiles for both P0 and P15 samples, as well as comparable total heat release (THR). The only appreciable difference was the ignition delay (20–22 s vs. 5–7 s) when fire development was driven solely by the self-combustion of volatile gases evolved from the surface (no trigger). Mass loss trends aligned with the combustion profile and were comparable among all samples. These findings are consistent with previously reported polyurethane foams [82–84]. Tests were interrupted at 400 s, by which time the flames had already extinguished and the HRR had dropped to negligible values, with only a few remaining embers.

At the lower heat flux of 25 kW/m^2, flame development was delayed (11–13 s vs. 5–7 s), the peak heat release rate (pHRR) was reduced (~300 kW/m^2 vs. ~ 400 kW/m^2), and heat release was more broadly distributed over time, while the THR remained similar. This trend agrees with literature data on heat flux variations [85]. A flux of 25 kW/m^2 was insufficient to initiate self-combustion of flammable gases, and visible flames occurred only in the presence of an electric spark. In the absence of an external ignition source, the samples produced emitted smoke but did not sustain flaming combustion. As a result, the HRR curve lacked the abrupt increase typically observed in burning polymers, with a maximum of only ~14 kW/m^2, THR not exceeding 6 MJ/m^2, and a mass loss rate markedly lower than in flaming conditions.

Smoke production was also monitored to provide a comprehensive overview of the fire behaviour of the materials [86,87]. As shown in Fig. 15, under the heat flux of 35 kW/m^2, the P15 foam exhibits a smoke production behaviour nearly identical to that of the unmodified PU (P0). The smoke production rate (SPR) and the total smoke production (TSP)

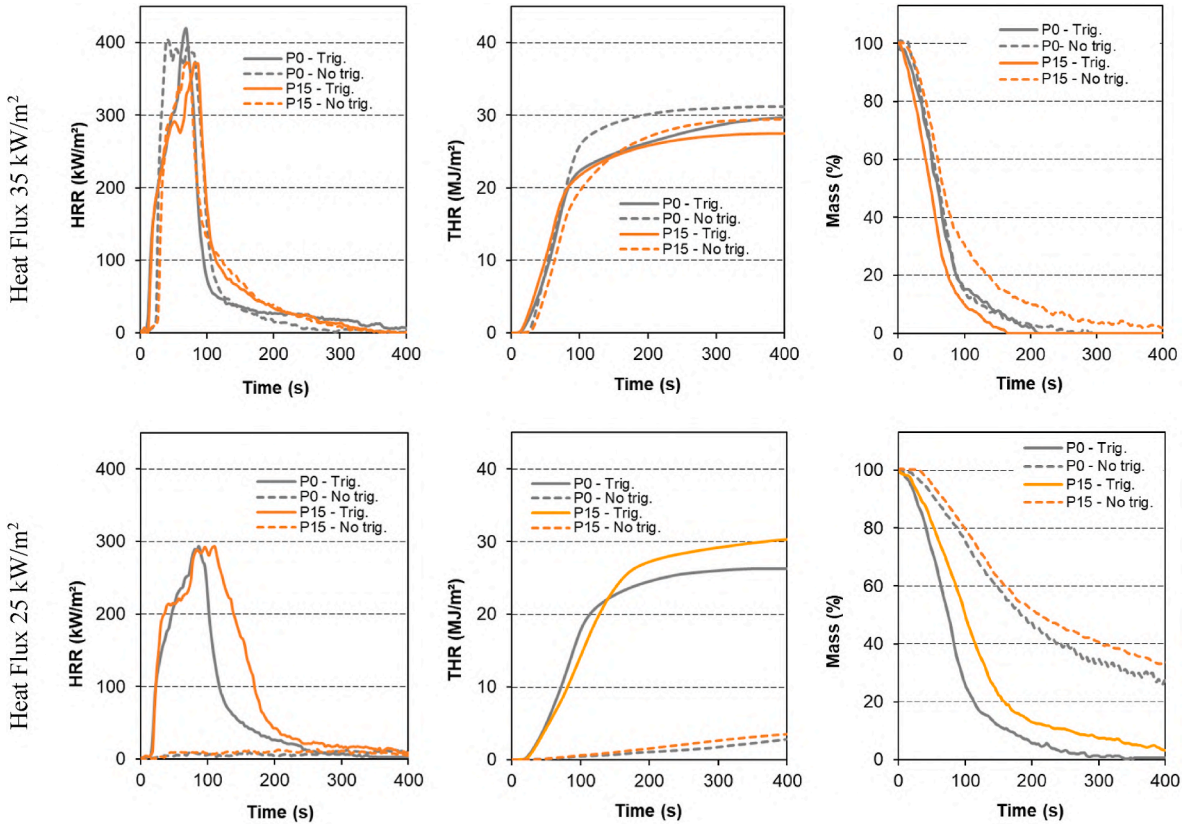

Fig. 14. Cone-calorimeter test results carried out under 35 kW/m^2 (top row) and 25 kW/m^2 (bottom row) heat flux. From left to right: Heat Release Rate (HRR), Total Heat Release (THR), and specimen mass trends over time.

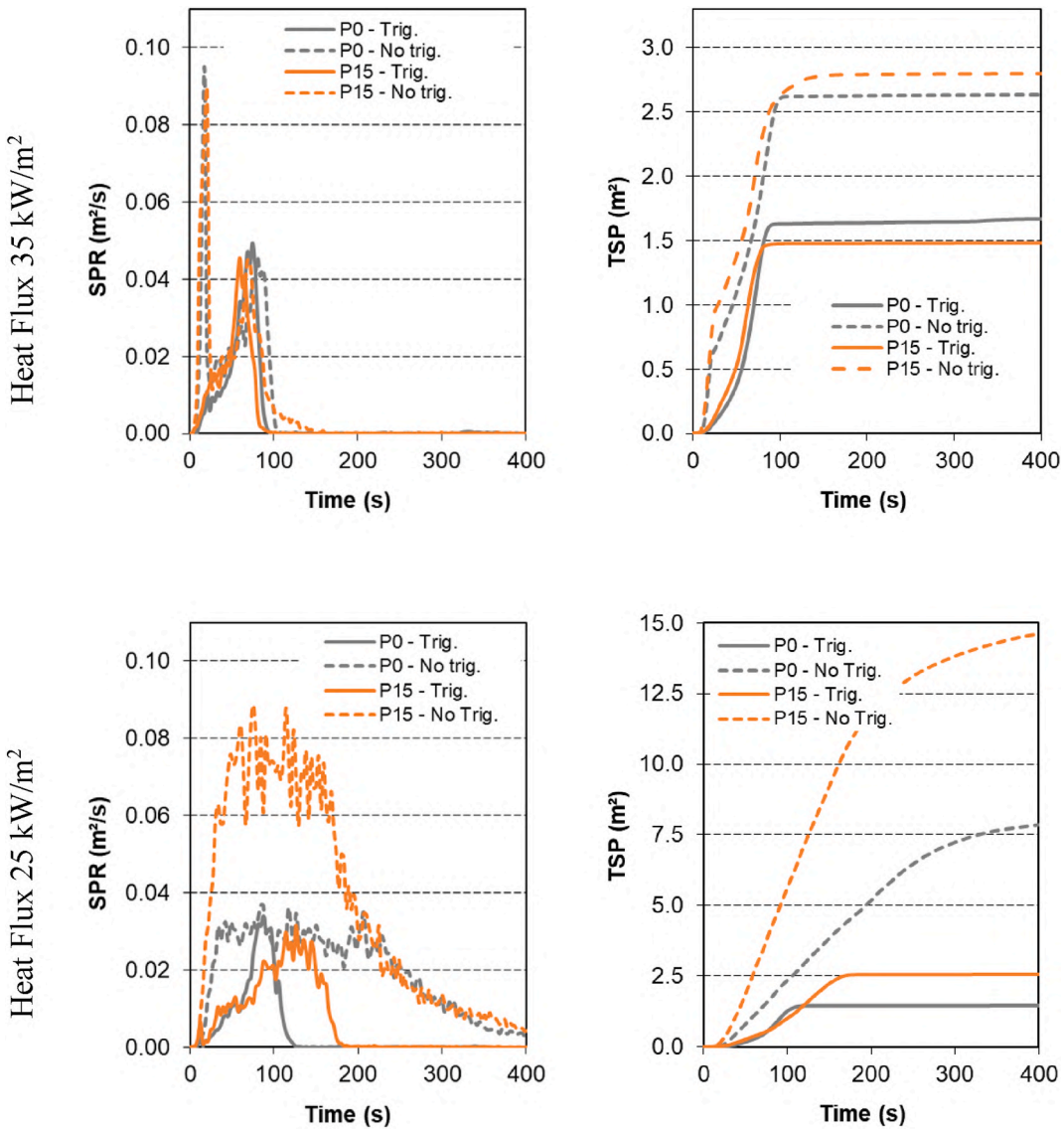

Fig. 15. Smoke evaluation by cone-calorimeter test carried out under 35 kW/m^2 (top row) and 25 kW/m^2 (bottom row) heat flux. Left: Smoke Production Rate (SPR); right: Total Smoke Production (TSP).

trends are comparable for both materials. However, a difference emerges between samples tested with and without the ignition trigger. The absence of a trigger produces a pronounced peak just a few seconds from the start of the test (maximum peak in SPR traces), corresponding to a high rate of smoke production. Then, after burning of the sample, the SPR reduces. The initial peak, associated with a high SPR, is absent in the case of samples tested with the ignition trigger. In terms of TSP, the smoke produced is almost halved in the case of heat exposure with the trigger. Such smoke reduction can be attributed to the early fire development compared with the samples that experienced spontaneous combustion. The smoke production of samples irradiated with 25 kW/m^2 is quite different: the presence of PCM leads to an increase in the smoke production, especially when the samples are allowed to self-ignite.

Overall, the addition of PCM (P15) did not significantly affect HRR and THR with respect to the virgin foam (P0), despite the intrinsic flammability of paraffin. This outcome is explained by the encapsulation of the PCM in a glass shell, which provides a protective barrier. Moreover, silica, the main component of the shell, is known to act as a flame retardant [88–92]. In general, silica creates a protective thermal barrier by insulating the flammable polymer matrix from heat [91], besides the formation of a char layer which, again, forms a physical barrier preventing combustion [93]. This barrier, promoted by silica, is also effective for the PCM particles under examination. Indeed, the paraffinic material is insulated by the silica shell, making the PCM material more thermally stable [94], and providing a physical barrier that reduces heat transfer to the core. This means that the silica shell reduces the rate at which heat reaches the inner material, thereby delaying its ignition and, consequently, limiting the spread of fire. Since the particle's core is made of high-flammable paraffin, it is not possible to avoid its burning; however, silica is able to counterbalance the paraffin's negative effect on the material flammability, leading to an overall "neutral" effect on the flame behaviour of the PCM-modified PU foams.

4. Conclusions

This study reports the development of sustainable flexible polyurethane (PU) composite foams with integrated thermal regulation capabilities for energy storage and insulation applications. In particular, it investigates the synergistic integration between silica-shell/paraffinic-core phase change materials (PCMs) and 80 wt% bio-based PU derived from waste cooking oils (WCO), evaluating their compatibility and

performance in the fabrication of flexible PU-PCM panels.

The key findings are as follows.

- PU-PCM panels were successfully produced using a direct PCM integration method. The PCM was effectively incorporated, exhibiting consistent phase change behaviour and enhanced energy storage capacity (up to 26.2 J/g) at the highest PCM content (15 phr). This enthalpy value aligns with previously reported data for petroleum-based polyurethane foams and polymer-based PCMs at 15 phr content. The encapsulation efficiency aligned with the theoretical PCM content introduced before PU foaming, with minimal particle segregation and no evidence of leakage.
- PU-PCM samples exhibited thermal stability up to 200 °C. The degradation behaviour and FTIR spectra of both virgin and PCM-containing panels were comparable, suggesting complete encapsulation of the PCM within the PU matrix. The addition of PCM did not significantly affect the fire performance under both 35 and 25 kW/m^2, with or without ignition source. This is likely due to a balance between the flammability of paraffinic core and the flame-retardant effect of the silica shell of the PCM microcapsules.
- PCM microcapsules were uniformly distributed within the PU matrix, predominantly accumulating at the cell strut joints. This resulted in a slight distortion and reduction in cell dimensions (from 200 to 500 to 100–450 μm) while increasing panel density (from 128 to 157 kg/m^3, corresponding to a 23 % rise). The incorporation of PCM enhanced the structural support, strength, and rigidity of the material while reducing its elasticity. Consequently, compression force deflection (CFD) increased from 85.5 kPa for virgin PU to 234.8 kPa with the addition of 15 phr PCM.
- Fatigue tests demonstrated the ability of the developed panels to withstand cyclic loading, with a reduction of dynamic stress to 25 % deformation that decreased with load-bearing cycles. The incorporation of PCM resulted in increased dynamic stress due to enhanced stiffness, leading to steeper polymer relaxation curves with higher PCM content and lower temperatures. DSC analysis conducted before and after fatigue tests confirmed negligible enthalpy hysteresis (±0.26 J/g) and stable phase-change temperatures (±0.1 °C), highlighting the resilience of the panels to thermal and mechanical stresses while maintaining energy storage capacity.
- The thermal conductivity of virgin foam increased linearly with temperature from 46.15 mW/m·K (20 °C) to 47.81 mW/m·K (50 °C). The panel with the highest PCM content exhibited a slightly higher thermal conductivity, ranging from 48.44 to 48.58 mW/m·K, due to the silica-based conductive PCM shell. The nearly constant thermal conductivity of the PCM-based panel with temperature is likely due to a balance between intrinsic temperature dependence and reduced conductivity near the solid-liquid phase transition (T_m = 36 °C). Furthermore, PCM-containing panels showed lower thermal diffusivity than the virgin foam, making them particularly suitable for transient thermal regimes where damping of temperature fluctuations is required.

The results demonstrate that the developed bio-based PU flexible panels incorporating PCMs are promising for applications in transportation and construction, where lightweight, insulating, and flame-retardant properties are required. The proposed PCM-loaded PU foams exhibit improved sustainability, along with enhanced thermal and mechanical performance, compared to conventional petrochemical PU panels and flammable PCMs. Furthermore, this strategy is consistent with circular economy principles, as it promotes resource recovery by valorising end-of-life WCO within a sustainable recycling chain.

Future work should concentrate on the evaluation of long-term stability and ageing behaviour of PU-PCM composites to ensure reliable performance over their service life. Additional investigations will address the incorporation of higher PCM contents (>15 phr) and the optimisation of reagents and additives. This approach is expected to further enhance the thermal energy storage capacity of the PU-PCM system, while maintaining foam flexibility and integrity, thereby broadening their potential applicability. Moreover, the use of fully bio-based PCMs derived from vegetable oils would further increase the overall sustainability of the resulting composite foams. The proposed utilisation of waste cooking oil (WCO) as the primary feedstock for PU-PCM panel production will also be evaluated in a forthcoming study through Life Cycle Assessment (LCA) to quantify its environmental impact.

CRediT authorship contribution statement

Damiano Rossi: Writing – original draft, Methodology, Investigation, Funding acquisition, Formal analysis, Conceptualization. **Irene Anguillesi:** Visualization, Validation, Investigation, Data curation. **Emanuele Maccaferri:** Investigation, Funding acquisition, Formal analysis. **Alekos Ioannis Garivalis:** Investigation, Formal analysis. **Ester D'Accardi:** Investigation, Formal analysis. **Davide Palumbo:** Investigation, Funding acquisition. **Maria Michela Dell'Anna:** Writing – review & editing, Supervision, Resources. **Daniele Testi:** Writing – review & editing, Supervision, Resources. **Loris Giorgini:** Writing – review & editing, Supervision, Resources. **Maurizia Seggiani:** Writing – review & editing, Supervision, Resources, Project administration, Conceptualization.

Funding sources

This research was funded by the European Union - Next Generation EU (National Sustainable Mobility Centre). CN00000023. Italian Ministry of University and Research Decree n. 1033-17/06/2022. Spoke 11 - Innovative Materials & Lightweighting - Scalability Project "ECO-FRIEND" and Flagship A "CO-SMART".

Declaration of competing interest

The authors declare that they have no known competing financial interests or personal relationships that could have appeared to influence the work reported in this paper.

Acknowledgements

The authors would like to acknowledge Covestro AG (Germany) and Evonik Industries AG (Germany) for generously providing Desmodur® CQ N7300 and the foaming additives, respectively. The authors appreciate the cooperation of Encapsys LLC (US) for kindly providing the phase change microcapsules.

Data availability

Data will be made available on request.

References

[1] H. Dong, S. Li, Z. Jia, Y. Luo, Y. Chen, J. Jiang, S. Ji, A review of polyurethane foams for multi-functional and high-performance applications, Polymers 16 (2024) 3182, https://doi.org/10.3390/polym16223182.
[2] A. Menon, P. Sreeram, A. Vinod, V. Naiker, M.V. Nandana, D.A. David, S. P. Sasidharan, P. Raghavan, Polyurethane (PU): structure, properties, and applications, in: Handbook of Thermosetting Foams, Aerogels, and Hydrogels, Elsevier, 2024, pp. 67–92.
[3] J.O. Akindoyo, M.D.H. Beg, S. Ghazali, M.R. Islam, N. Jeyaratnam, A.R. Yuvaraj, Polyurethane types, synthesis and applications – a review, RSC Adv. 6 (2016) 114453–114482, https://doi.org/10.1039/C6RA14525F.
[4] C.A. Ikutegbe, M.M. Farid, Application of phase change material foam composites in the built environment: a critical review, Renew. Sustain. Energy Rev. 131 (2020) 110008, https://doi.org/10.1016/j.rser.2020.110008.
[5] S. Sarkar, S. Mestry, S.T. Mhaske, Developments in phase Change Material (PCM) doped energy efficient polyurethane (PU) foam for perishable food cold-storage applications: a review, J. Energy Storage 50 (2022) 104620, https://doi.org/10.1016/j.est.2022.104620.

[6] P. GaneshKumar, G. Praveen Kumar, V. Sivalingam, S. Divya, T.H. Oh, Revolutionizing microelectronics cooling: thermal management with nano-enhanced PCMs, hybrid cooling, conductive foams, and porous structures, Renew. Sustain. Energy Rev. 222 (2025) 115954, https://doi.org/10.1016/j.rser.2025.115954.
[7] Q. Ma, M. Yang, X. Ye, Z. Du, X. Cheng, H. Wang, D. Xu, X. Du, Flexible Ti3C2Tx MXene/Polyolefin-Based phase change foaming film with solar-thermal conversion and sensitive motion detection for wearable thermal ManagementArticle link copied, Ind. Eng. Chem. Res. 64 (2025) 9722–9733, https://doi.org/10.1021/acs.iecr.5c00471.
[8] J. Wang, H. Yue, Z. Du, X. Cheng, H. Wang, X. Du, Highly flexible phase-change film with solar thermal storage and sensitive motion detection for wearable thermal management, Chem. Eng. J. 466 (2023) 143334, https://doi.org/10.1016/j.cej.2023.143334.
[9] A.I. Garivalis, D. Rossi, M. Seggiani, D. Testi, Review beyond water : physical and heat transfer properties of phase change slurries for thermal energy storage, Cell Rep. Phys. Sci. (2024) 101905, https://doi.org/10.1016/j.xcrp.2024.101905.
[10] A. Nandy, Y. Houl, W. Zhao, N.A. D'Souza, Thermal heat transfer and energy modeling through incorporation of phase change materials (PCMs) into polyurethane foam, Renew. Sustain. Energy Rev. 182 (2023) 113410, https://doi.org/10.1016/j.rser.2023.113410.
[11] M. Izadi, I. Pop, S.A. Shehzad, F. Alqurashi, M.H. Mohamed, A. Hajjar, I. Mahariq, Comprehensive review of optimization strategies for phase change materials: techniques, applications, and challenges in thermal storage systems, Int. Commun. Heat Mass Tran. 166 (2025) 109123, https://doi.org/10.1016/j.icheatmasstransfer.2025.109123.
[12] N. Sarier, E. Onder, Thermal characteristics of polyurethane foams incorporated with phase change materials, Thermochim. Acta 454 (2007) 90–98, https://doi.org/10.1016/j.tca.2006.12.024.
[13] Ming You, Xing-xiang Zhang, Xue-chen Wang, Li Zhang, Wen Wen, Effects of type and contents of microencapsuled N-Alkanes on properties of soft polyurethane foams, Thermochim. Acta 500 (2010) 69–75, https://doi.org/10.1016/j.tca.2009.12.013.
[14] U.R. Mahajan, I. Emmanuel, A.S. Rao, S.T. Mhaske, Development of rigid polyurethane foam incorporating phase change material for a low-temperature thermal energy storage application, Polym. Int. 72 (2023) 490–499, https://doi.org/10.1002/pi.6492.
[15] E. Vatankhah, M. Abasnezhad, M. Nazerian, M. Barmar, A. Partovinia, Thermal energy storage and mechanical performance of composites of rigid polyurethane foam and phase change material prepared by one-shot synthesis method, J. Polym. Res. 29 (2022), https://doi.org/10.1007/s10965-022-02911-z.
[16] C. Castellón, M. Medrano, J. Roca, L.F. Cabeza, M.E. Navarro, A.I. Fernández, A. Lázaro, B. Zalba, Effect of microencapsulated phase change material in sandwich panels, Renew. Energy 35 (2010) 2370–2374, https://doi.org/10.1016/j.renene.2010.03.030.
[17] C. Amaral, S.C. Pinto, T. Silva, F. Mohseni, J.S. Amaral, V.S. Amaral, P.A.A. P. Marques, A. Barros-Timmons, R. Vicente, Development of polyurethane foam incorporating phase change material for thermal energy storage, J. Energy Storage 28 (2020) 101177, https://doi.org/10.1016/j.est.2019.101177.
[18] A.T. Naikwadi, A.B. Samui, P.A. Mahanwar, Fabrication and experimental investigation of microencapsulated eutectic phase change material-integrated polyurethane sandwich Tin Panel composite for thermal energy storage in buildings, Int. J. Energy Res. 45 (2021) 20783–20794, https://doi.org/10.1002/er.7138.
[19] F. Galvagnini, A. Dorigato, F. Valentini, V. Fiore, M. La Gennusa, A. Pegoretti, Multifunctional polyurethane foams with thermal energy Storage/Release capability, J. Therm. Anal. Calorim. 147 (2022) 297–313, https://doi.org/10.1007/s10973-020-10367-w.
[20] G. Fredi, E. Boso, A. Sorze, A. Pegoretti, Multifunctional sandwich composites with optimized phase change material content for simultaneous structural and thermal performance, Compos Part A Appl Sci Manuf 186 (2024) 108382, https://doi.org/10.1016/j.compositesa.2024.108382.
[21] C. Arumugam, S. Shaik, A. Roy, K.J. Kontoleon, E. Cuce, A.H. Shaik, S. Chakraborty, M. Alwetaishi, P.M. Cuce, M. Gupta, Analysis of the benefits of adopting roof sandwich panels integrated with PCM versus PUR to mitigate energy costs and carbon dioxide emissions, J. Energy Storage 77 (2024) 109947, https://doi.org/10.1016/j.est.2023.109947.
[22] Y. Yuan, Q. Guo, L. Xu, W. Wang, Rigid polyurethane foam derived from renewable sources: research progress, property enhancement, and future prospects, Molecules 30 (2025) 678, https://doi.org/10.3390/molecules30030678.
[23] J.A.M. Vargas, K.S. Mandrekar, R. Echemendía, A.C.B. Burtoloso, Innovations in isocyanate synthesis for a sustainable future, Org. Biomol. Chem. 23 (2025) 487–505, https://doi.org/10.1039/D4OB01598C.
[24] M.A. Sawpan, Polyurethanes from vegetable oils and applications: a review, J. Polym. Res. 25 (2018) 184, https://doi.org/10.1007/s10965-018-1578-3.
[25] D.S. Kaikade, A.S. Sabnis, Polyurethane foams from vegetable oil-based polyols: a review, Polym. Bull. 80 (2023) 2239–2261, https://doi.org/10.1007/s00289-022-04155-9.
[26] Z. Petrovic, Polyurethanes from vegetable oils, Polym. Rev. 48 (2008) 109–155, https://doi.org/10.1080/15583720701834224.
[27] M. Cappello, S. Filippi, D. Rossi, P. Cinelli, I. Anguillesi, C. Camodeca, E. Orlandini, G. Polacco, M. Seggiani, Waste-Cooking-Oil-Derived polyols to produce new sustainable rigid polyurethane foams, Sustainability 16 (2024) 9456, https://doi.org/10.3390/su16219456.
[28] D. Rossi, I. Anguillesi, M. Cappello, M.M. Dell'Anna, M. Seggiani, Novel synthesis of flexible polyurethane foams with high bio-based content derived from waste cooking oil. Scientific Reports, Springer - In Press, 2025.
[29] Covestro, Technical Data Sheet Desmodur CQ N 7300, Available online: https://solutions.covestro.com/en/products/desmodur/desmodur-cq-ultra-n-7300_86667711-23651068?SelectedCountry=US.
[30] Vegetable oils consumption worldwide. 2023/2024, Available online: https://www.statista.com/statistics/263937/vegetable-oils-global-consumption/. (Accessed 9 May 2025).
[31] C.G. Lopresto, M.G. De Paola, V. Calabrò, Importance of the properties, collection, and storage of waste cooking oils to produce high-quality biodiesel – an overview, Biomass Bioenergy 189 (2024), https://doi.org/10.1016/j.biombioe.2024.107363.
[32] A. Mannu, M. Ferro, M.E. Di Pietro, A. Mele, Innovative applications of waste cooking oil as raw material, Sci. Prog. 102 (2019) 153–160, https://doi.org/10.1177/0036850419854252.
[33] M. Onn, M.J. Jalil, N.I.S. Mohd Yusoff, E.B. Edward, M.U. Wahit, A comprehensive review on chemical route to convert waste cooking oils to renewable polymeric materials, Ind. Crops Prod. 211 (2024) 118194, https://doi.org/10.1016/j.indcrop.2024.118194.
[34] N.V. Gama, C. Amaral, T. Silva, R. Vicente, J.A.P. Coutinho, A. Barros-Timmons, A. Ferreira, Thermal energy storage and mechanical performance of crude glycerol polyurethane composite foams containing phase change materials and expandable graphite, Materials 11 (2018), https://doi.org/10.3390/ma11101896.
[35] J. Giro-Paloma, M. Martínez, L.F. Cabeza, A.I. Fernández, Types, methods, techniques, and applications for Microencapsulated Phase Change Materials (MPCM): a review, Renew. Sustain. Energy Rev. 53 (2016) 1059–1075, https://doi.org/10.1016/j.rser.2015.09.040.
[36] C. Yang, L. Fischer, S. Maranda, J. Worlitschek, Rigid polyurethane foams incorporated with phase change materials: a state-of-the-art review and future research pathways, Energy Build. 87 (2015) 25–36, https://doi.org/10.1016/j.enbuild.2014.10.075.
[37] A. Serrano, A.M. Borreguero, I. Garrido, J.F. Rodríguez, M. Carmona, Reducing heat loss through the building envelope by using polyurethane foams containing thermoregulating microcapsules, Appl. Therm. Eng. 103 (2016) 226–232, https://doi.org/10.1016/j.applthermaleng.2016.04.098.
[38] C. Amaral, R. Vicente, V.M. Ferreira, T. Silva, Polyurethane foams with microencapsulated phase change material: comparative analysis of thermal conductivity characterization approaches, Energy Build. 153 (2017) 392–402, https://doi.org/10.1016/j.enbuild.2017.08.019.
[39] A. Tinti, A. Tarzia, A. Passaro, R. Angiuli, Thermographic analysis of polyurethane foams integrated with phase change materials designed for dynamic thermal insulation in refrigerated transport, Appl. Therm. Eng. 70 (2014) 201–210, https://doi.org/10.1016/j.applthermaleng.2014.05.003.
[40] S. Marchi, S. Pagliolico, G. Sassi, Characterization of panels containing micro-encapsulated phase change materials, Energy Convers. Manag. 74 (2013) 261–268, https://doi.org/10.1016/j.enconman.2013.05.027.
[41] R.A. Lawag, H.M. Ali, Phase change materials for thermal management and energy storage: a review, J. Energy Storage 55 (2022) 105602, https://doi.org/10.1016/j.est.2022.105602.
[42] N. Hammami, L. Liu, L. Trovalet, D. Bigot, B. Malet-Damour, J.P. Habas, Can vegetable oils be used as sustainable phase change materials for thermal energy storage in building? Mater. Today Sustain. 23 (2023) 100469 https://doi.org/10.1016/j.mtsust.2023.100469.
[43] M. Zadshir, B.-W. Kim, H. Yin, Bio-Based phase change materials for sustainable development, Materials 17 (2024) 4816, https://doi.org/10.3390/ma17194816.
[44] F.L. Rashid, M.A. Al-Obaidi, N.S. Dhaidan, A.K. Hussein, B. Ali, M.B. Ben Hamida, O. Younis, Bio-Based phase change materials for thermal energy storage and release: a review, J. Energy Storage 73 (2023) 109219, https://doi.org/10.1016/j.est.2023.109219.
[45] A. Ismail, J. Zhou, A. Aday, I. Davidoff, A. Odukomaiya, J. Wang, Microencapsulation of bio-based phase change materials with Silica coated inorganic shell for thermal energy storage, J. Build. Eng. 67 (2023) 105981, https://doi.org/10.1016/j.jobe.2023.105981.
[46] B. Kalidasan, A.K. Pandey, R. Saidur, B. Aljafari, A. Yadav, M. Samykano, Green synthesized 3D coconut shell Biochar/Polyethylene glycol composite as thermal energy storage material, Sustain. Energy Technol. Assessments 60 (2023) 103505, https://doi.org/10.1016/j.seta.2023.103505.
[47] B. Kalidasan, A.K. Pandey, R. Saidur, R. Kothari, K. Sharma, V.V. Tyagi, Eco-Friendly coconut Shell biochar based Nano-Inclusion for sustainable energy storage of binary eutectic salt hydrate phase change materials, Sol. Energy Mater. Sol. Cell. 262 (2023) 112534, https://doi.org/10.1016/j.solmat.2023.112534.
[48] T.K. Maiti, P. Dixit, A. Suhag, S. Bhushan, A. Yadav, N. Talapatra, S. Chattopadhyay, Advancements in organic and inorganic shell materials for the preparation of microencapsulated phase change materials for thermal energy storage applications, RSC Sustain. 1 (2023) 665–697, https://doi.org/10.1039/D2SU00116K.
[49] X. Chen, Z. Tang, Y. Chang, H. Gao, P. Cheng, Z. Tao, J. Lv, Toward tailoring chemistry of Silica-Based phase change materials for thermal energy storage, iScience 23 (2020) 101606, https://doi.org/10.1016/j.isci.2020.101606.
[50] M. Delgado, A. Lázaro, J. Mazo, B. Zalba, Review on phase change material emulsions and microencapsulated phase change material slurries: materials, heat transfer studies and applications, Renew. Sustain. Energy Rev. 16 (2012) 253–273, https://doi.org/10.1016/j.rser.2011.07.152.
[51] V. Pethurajan, S. Sivan, A.J. Konatt, A.S. Reddy, Facile approach to improve solar thermal energy storage efficiency using encapsulated sugar alcohol based phase

change material, Sol. Energy Mater. Sol. Cell. 185 (2018) 524–535, https://doi.org/10.1016/j.solmat.2018.06.007.
[52] Y. Zhu, S. Liang, K. Chen, X. Gao, P. Chang, C. Tian, J. Wang, Y. Huang, Preparation and properties of nanoencapsulated N-Octadecane phase change material with Organosilica shell for thermal energy storage, Energy Convers. Manag. 105 (2015) 908–917, https://doi.org/10.1016/j.enconman.2015.08.048.
[53] P. Sittisart, M.M. Farid, Fire retardants for phase change materials, Appl. Energy 88 (2011) 3140–3145, https://doi.org/10.1016/j.apenergy.2011.02.005.
[54] A. Sabbahi, J.M. Vergnaud, Absorption of water by polyurethane foam. Modelling and experiments, Eur. Polym. J. 29 (1993) 1243–1246, https://doi.org/10.1016/0014-3057(93)90155-9.
[55] V. Vand, Theory of viscosity of concentrated suspensions, Nature 155 (1945) 364–365, https://doi.org/10.1038/155364b0.
[56] A. Serrano, A.M. Borreguero, I. Garrido, J.F. Rodríguez, M. Carmona, The role of microstructure on the mechanical properties of polyurethane foams containing thermoregulating microcapsules, Polym. Test. 60 (2017) 274–282, https://doi.org/10.1016/j.polymertesting.2017.04.011.
[57] X. Zhang, Y. Fan, X. Tao, K. Yick, Crystallization and prevention of supercooling of microencapsulated N-Alkanes, J. Colloid Interface Sci. 281 (2005) 299–306, https://doi.org/10.1016/j.jcis.2004.08.046.
[58] S. Li, B. Dong, J. Wang, J. Li, T. Shen, H. Peng, X. Ling, Synthesis and characterization of mixed alkanes microcapsules with phase change temperature below ice point for cryogenic thermal energy storage, Energy 187 (2019) 115898, https://doi.org/10.1016/j.energy.2019.115898.
[59] D.K. Chattopadhyay, D.C. Webster, Thermal stability and flame retardancy of polyurethanes, Prog. Polym. Sci. 34 (2009) 1068–1133, https://doi.org/10.1016/j.progpolymsci.2009.06.002.
[60] F. Askari, M. Barikani, M. Barmar, F. Shokrolahi, M. Vafayan, Study of thermal stability and degradation kinetics of polyurethane–ureas by thermogravimetry, Iran. Polym. J. (Engl. Ed.) 24 (2015) 783–789, https://doi.org/10.1007/s13726-015-0367-7.
[61] S. Członka, A. Strąkowska, K. Strzelec, A. Kairytė, S. Vaitkus, Composites of rigid polyurethane foams and Silica Powder Filler enhanced with ionic liquid, Polym. Test. 75 (2019) 12–25, https://doi.org/10.1016/j.polymertesting.2019.01.021.
[62] M. Zieleniewska, M. Auguścik, A. Prociak, P. Rojek, J. Ryszkowska, Polyurethane-Urea substrates from rapeseed oil-based polyol for bone tissue cultures intended for application in tissue engineering, Polym. Degrad. Stabil. 108 (2014) 241–249, https://doi.org/10.1016/j.polymdegradstab.2014.03.010.
[63] Y. Jin, X. Hu, C. Wu, R. Zong, S. Liu, B. Shentu, Influence of palm oil-based polyols on the microstructure and properties of bio-based flexible polyurethane foams, Biomass Convers Biorefin 14 (2024) 32109–32119, https://doi.org/10.1007/s13399-023-04899-y.
[64] A.E. Coman, J. Peyrton, G. Hubca, A. Sarbu, A.R. Gabor, C.A. Nicolae, T. V. Iordache, L. Averous, Synthesis and characterization of renewable polyurethane foams using different biobased polyols from olive oil, Eur. Polym. J. 149 (2021) 110363, https://doi.org/10.1016/j.eurpolymj.2021.110363.
[65] J.A. de Haseth, J.E. Andrews, J.V. McClusky, R.D. Priester, M.A. Harthcock, B. L. Davis, Characterization of polyurethane foams by mid-infrared Fiber/FT-IR spectrometry, Appl. Spectrosc. 47 (1993) 173–179, https://doi.org/10.1366/0003702934048334.
[66] Y. Zhang, J. Zhang, X. Li, X. Wu, Preparation of Hydrophobic lauric Acid/SiO2 Shape-Stabilized phase change materials for thermal energy storage, J. Energy Storage 21 (2019) 611–617, https://doi.org/10.1016/j.est.2018.12.022.
[67] S. Ishak, S. Mandal, H.S. Lee, J.K. Singh, PH-Controlled synthesis of sustainable lauric Acid/SiO2 phase change material for scalable thermal energy storage, Sci. Rep. 11 (2021) 1–15, https://doi.org/10.1038/s41598-021-94571-0.
[68] S. Wang, P. Qin, X. Fang, Z. Zhang, S. Wang, X. Liu, A novel sebacic Acid/Expanded graphite composite phase change material for solar thermal medium-temperature applications, Sol. Energy 99 (2014) 283–290, https://doi.org/10.1016/j.solener.2013.11.018.
[69] A.M. Borreguero, J.F. Rodríguez, J.L. Valverde, R. Arevalo, T. Peijs, M. Carmona, Characterization of rigid polyurethane foams containing microencapsulated rubitherm® RT27: catalyst effect. Part II, J. Mater. Sci. 46 (2011) 347–356, https://doi.org/10.1007/s10853-010-4824-6.
[70] I. Javni, W. Zhang, V. Karajkov, Z.S. Petrovic, V. Divjakovic, Effect of Nano- and Micro-Silica fillers on polyurethane foam properties, J. Cell. Plast. 38 (2002) 229–239, https://doi.org/10.1177/0021955X02038003139.
[71] A.B. Francés, M.V.N. Bañón, Effect of Silica nanoparticles on polyurethane foaming process and foam properties, IOP Conf. Ser. Mater. Sci. Eng. 64 (2014), https://doi.org/10.1088/1757-899X/64/1/012020.
[72] M. Ates, S. Karadag, A.A. Eker, B. Eker, Polyurethane foam materials and their industrial applications, Polym. Int. 71 (2022) 1157–1163, https://doi.org/10.1002/pi.6441.
[73] J. Wang, C. Zhang, Y. Deng, P. Zhang, A review of research on the effect of temperature on the properties of polyurethane foams, Polymers 14 (2022) 4586, https://doi.org/10.3390/polym14214586.
[74] W. Leng, B. Pan, Thermal insulating and mechanical properties of cellulose nanofibrils modified polyurethane foam composite as structural insulated material, Forests 10 (2019) 200, https://doi.org/10.3390/f10020200.
[75] K. Uhlig, Discovering Polyurethanes, Carl Hanser Verlag, Munich, 1999.
[76] S. Patra, P.M. Ajayan, T.N. Narayanan, Dynamic mechanical analysis in materials science: the novice's tale, Oxford Open Materials Science 1 (2020), https://doi.org/10.1093/oxfmat/itaa001.
[77] P. Cimavilla-Román, M. Santiago-Calvo, M.Á. Rodríguez-Pérez, Dynamic mechanical analysis during polyurethane foaming: relationship between modulus Build-up and reaction kinetics, Polym. Test. 103 (2021) 107336, https://doi.org/10.1016/j.polymertesting.2021.107336.
[78] S. Demirel, B. Ergun Tuna, Evaluation of the cyclic fatigue performance of polyurethane foam in different density and category, Polym. Test. 76 (2019) 146–153, https://doi.org/10.1016/j.polymertesting.2019.03.019.
[79] Z. Chen, G. Fang, Preparation and heat transfer characteristics of microencapsulated phase change material slurry: a review, Renew. Sustain. Energy Rev. 15 (2011) 4624–4632, https://doi.org/10.1016/j.rser.2011.07.090.
[80] A.F. Baguian, S.K. Ouiminga, C. Longuet, A.-S. Caro-Bretelle, S. Corn, A. Bere, R. Sonnier, Influence of density on foam collapse under burning, Polymers 13 (2020) 13, https://doi.org/10.3390/polym13010013.
[81] Y. Wang, W. Kang, C. Chen, X. Zhang, L. Yang, X. Chen, G. Cui, Y. Zhang, F. Zhang, S. Li, Combustion behaviour and dominant shrinkage mechanism of flexible polyurethane foam in the cone calorimeter Test, J Hazard Mater 365 (2019) 395–404, https://doi.org/10.1016/j.jhazmat.2018.11.027.
[82] O. Ugo-Okeke, D. Torvi, Effects of incident heat flux on heat release rates and temperatures in cone calorimeter tests of polyurethane foam, Fire Mater. 48 (2024) 699–714, https://doi.org/10.1002/fam.3224.
[83] M. Checchin, C. Cecchini, B. Cellarosi, F.O. Sam, Use of cone calorimeter for evaluating fire performances of polyurethane foams, Polym. Degrad. Stabil. 64 (1999) 573–576, https://doi.org/10.1016/S0141-3910(98)00131-1.
[84] M. Günther, A. Lorenzetti, B. Schartel, Fire phenomena of rigid polyurethane foams, Polymers 10 (2018) 1166, https://doi.org/10.3390/polym10101166.
[85] X.-F. Liu, X. Luo, B.-W. Liu, H.-Y. Zhong, D.-M. Guo, R. Yang, L. Chen, Y.-Z. Wang, Toughening epoxy resin using a liquid crystalline elastomer for versatile application, ACS Appl. Polym. Mater. 1 (2019) 2291–2301, https://doi.org/10.1021/acsapm.9b00319.
[86] X. Zhang, Q. Guan, Q. Xiao, Z. Wang, H. Xie, Enhanced thermal and mechanical properties of flame-retardant expandable Graphite modified silk fibroin-based rigid polyurethane foam, Case Stud. Therm. Eng. 64 (2024) 105418, https://doi.org/10.1016/j.csite.2024.105418.
[87] X. Zhang, X. Qu, Q. Guan, R. Li, Z. Wang, H. Xie, Rigid polyurethane foam with improved thermal stability and flame retardancy modified by barium phytate and zinc oxide, Case Stud. Therm. Eng. 72 (2025) 106261, https://doi.org/10.1016/j.csite.2025.106261.
[88] M. Song, J. Choi, D. Kim, H. Han, S. Jeon, Eco-Friendly wood composites with enhanced mechanical strength and flame retardancy, J. Build. Eng. 104 (2025) 112260, https://doi.org/10.1016/j.jobe.2025.112260.
[89] L. Bo, G. Hua, J. Xian, S. Zeinali Heris, E. Erfani Farsi Eidgah, M.M. Ghafurian, Y. Orooji, Recent remediation strategies for flame retardancy via nanoparticles, Chemosphere 354 (2024) 141323, https://doi.org/10.1016/j.chemosphere.2024.141323.
[90] B. Paul, A. Mahmud-Ali, M. Lenninger, S. Eberle, I. Bernt, D. Mayer, T. Bechtold, Silica incorporated cellulose fibres as green concept for textiles with reduced flammability, Polym. Degrad. Stabil. 195 (2022) 109808, https://doi.org/10.1016/j.polymdegradstab.2021.109808.
[91] L. Yan, Z. Xu, X. Wang, Influence of Nano-Silica on the flame retardancy and smoke suppression properties of transparent intumescent fire-retardant coatings, Prog. Org. Coating 112 (2017) 319–329, https://doi.org/10.1016/j.porgcoat.2017.07.017.
[92] T. Kashiwagi, J.W. Gilman, K.M. Butler, R.H. Harris, J.R. Shields, A. Asano, Flame retardant mechanism of Silica Gel/Silica, Fire Mater. 24 (2000) 277–289, https://doi.org/10.1002/1099-1018(200011/12)24:6<277::AID-FAM746>3.0.CO;2-A.
[93] B. Qu, R. Xie, Intumescent char structures and flame-retardant mechanism of expandable graphite-based Halogen-free flame-retardant Linear low density polyethylene blends, Polym. Int. 52 (2003) 1415–1422, https://doi.org/10.1002/pi.990.
[94] R.J. Adnin, H.-S. Lee, Advancing thermal energy storage: synthesis and thermal performance of Silica-Encapsulated paraffin PCMs, Molecules 30 (2025) 1698, https://doi.org/10.3390/molecules30081698.